Melatonin ameliorates circadian rhythm disruption induced erectile dysfunction by inhibiting oxidative stress mediated pyroptosis via Nrf2/HO-1 axis

QINGTAO YANG[1*], WEI LI[1*], QI YU[2*], JIANG SHI[1], LU YANG[3], JUN QIAO[1], XI WEI[1], CHANGSHI GU[1], FA SUN[1] and TAO LI[1]

[1]Department of Urology, The Affiliated Hospital of Guizhou Medical University, Guiyang, Guizhou 550004, P.R. China; [2]Department of Reproductive Center, Affiliated Hospital of Guizhou Medical University, Guiyang, Guizhou 550004, P.R. China; [3]Department of Urology and Institute of Urology, West China Hospital, Sichuan University, Chengdu, Sichuan 610041, P.R. China

Received December 4, 2025; Accepted May 21, 2026

DOI: 10.3892/ijmm.2026.5888

Abstract. Circadian rhythm disruption (CRD) is highly prevalent in modern society and contributes to numerous disorders, including erectile dysfunction (ED). Melatonin (MT) possesses well-established functions in regulating circadian rhythm and demonstrating antioxidant ability; however, whether MT could preserve CRD-induced ED and the underlying mechanism has never been reported. A rat model with CRD-induced ED was designed by changing light-dark cycle (2h:2h alteration) and then intraperitoneally administering MT with low (5 mg/kg/day) and high (10 mg/kg/day) dosages. A total of 4 weeks later, rats' erectile function was measured and penile corpus cavernosum was subsequently harvested for analysis. In addition, bioinformatics analysis was performed to filter the possible molecular target, while lipopolysaccharide (LPS)-treated human umbilical vein endothelial cells (HUVECs) were selected to imitate CRD stimulation *in vivo* to further verify the underlying molecular mechanism. CRD significantly reduced rats' maximal intracavernous pressure (mICP) and mICP/mean arterial pressure (MAP) ratio, it also inhibited endothelial nitric oxide synthase/nitric oxide/cyclic guanosine monophosphate concentrations and injured normal penile corpus cavernosum structure, suggesting rats' normal erectile function was impaired; however, this CRD-induced ED was preserved by MT. The *in vivo* and *in vitro* experiments respectively proved that CRD increased oxidative stress of penile corpus cavernosum and HUVECs by reducing nuclear factor erythroid 2-related factor 2 (Nrf2)/heme oxygenase-1 (HO-1) production, while MT increased Nrf2/HO-1 to inhibit the oxidative stress. Meanwhile, CRD promoted pyroptosis in penile corpus cavernosum and HUVECs by increasing NLR family pyrin domain containing 3 (NLRP3) activation, which was relieved by MT through the attenuation of oxidative stress. Moreover, the reactive oxygen species inhibitor (NAC) inhibited CRD-induced pyroptosis of HUVECs to preserve normal function, which confirmed that MT alleviated NLRP3-mediated pyroptosis to preserved CRD-induced ED by reducing oxidative stress. In conclusion, it was demonstrated that CRD-induced ED by triggering an oxidative stress-pyroptosis cascade. Conversely, MT treatment effectively counteracts this pathology by activating the Nrf2/HO-1 pathway to suppress oxidative stress, thereby attenuating NLRP3-mediated pyroptosis and ultimately restoring erectile function. These results provide the first systematic evidence for the central role of the oxidative stress-pyroptosis axis in CRD-induced ED, establishing a solid theoretical foundation for MT as a promising therapeutic strategy for CRD-related ED.

Introduction

Erectile dysfunction (ED) is a prevalent male disorder (1), with an estimated 332 million cases worldwide by 2026 (2), severely impairing the physical and mental health of both patients and their partners. Although phosphodiesterase type 5 inhibitors (PDE5is) represent a milestone in ED treatment (3), their use is limited by contraindications and suboptimal efficacy in refractory ED (4). Therefore, identifying modifiable risk factors and exploring novel therapeutic strategies is urgently needed. In recent years, modern lifestyles, including shift work, sleep deprivation, frequent jet lag and excessive artificial light exposure, have become increasingly common, and these factors can disrupt the body's internal timing system, a condition termed circadian rhythm disruption (CRD) (5,6). Emerging epidemiological evidence indicates that CRD has become a growing concern in the field of male reproductive health and is closely

Correspondence to: Professor Tao Li or Dr Fa Sun, Department of Urology, The Affiliated Hospital of Guizhou Medical University, 9 Beijing Road, Guiyang, Guizhou 550004, P.R. China
E-mail: litaolitao163361@163.com
E-mail: sfgmc@sina.com

*Contributed equally

Key words: circadian rhythm disruption, erectile dysfunction, melatonin, oxidative stress, pyroptosis

associated with the development and progression of ED (7,8). Although previous studies by the authors have confirmed that CRD significantly impairs erectile function in rats (9,10), the underlying mechanisms remain largely unclear.

Notably, CRD may promote the development of ED through two distinct pathways. First, CRD can indirectly increase the risk of metabolic and cardiovascular diseases, which are well-established independent risk factors for ED (7,8). Second, CRD may directly impair erectile function through mechanisms independent of the aforementioned metabolic complications, such as inducing endothelial CRD, oxidative stress, and penile corpus cavernosum tissue damage (11,12). Although the indirect pathway has been extensively studied, the direct pathogenic role of CRD in ED remains poorly understood. Therefore, the present study aims to focus on the direct pathogenic effects of CRD, using a rigorously controlled animal model (excluding significant changes in body weight and serum testosterone levels, as shown in Figs. S1 and S2) to minimize confounding influences from systemic metabolic factors.

As a core regulator of systemic redox homeostasis, the circadian rhythm controls the expression of antioxidant enzymes [for example, superoxide dismutase (SOD), glutathione peroxidase (GPx) and catalase (CAT)] through core clock genes (for example, Clock, Bmal1, Per and Cry), generating rhythmic fluctuations in antioxidant capacity to counterbalance the peaks of metabolically produced reactive oxygen species (ROS) (9,13). CRD disrupts this synchrony, leading to impaired ROS clearance and accumulation of oxidative products, thereby inducing a state of 'rhythmic oxidative stress dysregulation'. In the penile corpus cavernosum, this imbalance directly damages endothelial cells, suppresses the endothelial nitric oxide synthase (eNOS)-nitric oxide (NO)-cyclic guanosine monophosphate (cGMP) pathway, and promotes fibrosis. More critically, persistently elevated ROS are potent activators of the NLR family pyrin domain containing 3 (NLRP3) inflammasome (14); its activation triggers Caspase-1-mediated pyroptosis, resulting in cell membrane rupture and the release of large amounts of pro-inflammatory cytokines (for example, IL-1β and IL-18), which further amplify local inflammation and tissue damage (15-18). Thus, oxidative stress not only directly impairs endothelial function but also initiates a 'oxidative stress-pyroptosis' vicious cycle, exacerbating structural damage to the corpus cavernosum. Ultimately, CRD constitutes a core pathogenic axis from circadian disruption to ED by disrupting the local rhythmic balance of oxidative stress and activating the pyroptosis cascade.

Melatonin (MT), a key synchronizer of the endogenous circadian rhythm, regulates circadian physiological processes such as sleep-wake cycles through MT1/MT2 receptors (19), providing a theoretical basis for intervening in CRD-related pathologies. Beyond its circadian regulatory function, MT and its metabolites possess potent free radical-scavenging abilities and can activate the Nrf2/HO-1 pathway to enhance endogenous antioxidant defense (20), while also inhibiting NLRP3 inflammasome-mediated pyroptosis (21), which aligns closely with the 'oxidative stress-pyroptosis' axis investigated in the present study. Previous studies have demonstrated that MT exerts protective effects in various ED models, including diabetes-induced ED, cavernous nerve injury, and age-related ED, as well as in testicular ischemia-reperfusion injury and varicocele (22,23). These lines of evidence support the therapeutic potential of MT against CRD-induced ED, providing a solid rationale for the present study.

Previous studies by the authors have shown that CRD induced by an altered light-dark cycle (2 h:2 h) significantly impairs erectile function in rats, as evidenced by reduced intracavernous pressure and decreased activity of the eNOS-NO-cGMP pathway (9,10). However, these earlier investigations were primarily observational and did not elucidate the underlying molecular mechanisms. Specifically, it remains unclear how CRD disrupts endothelial homeostasis, which downstream signaling pathways mediate the damage, and whether MT can intervene in this process. The present study was designed to fill these mechanistic gaps by systematically investigating the role of oxidative stress and pyroptosis in CRD-induced ED and by delineating the molecular basis of MT's therapeutic effects.

Materials and methods

Animal experimental design. A total of 24 male Sprague-Dawley (SD) rats (12-weeks old; weight, ~200 g) were obtained from the Experimental Animal Center of Guizhou Medical University. The animal protocols were approved by the Animal Ethics Committee of Guizhou Medical University (approval no. 2402989; Guiyang, China). All rats were acclimatized for 1 week under controlled temperature conditions at 22-25˚C, 55-70% humidity, and received unrestricted access to food and water. They were divided into one Control group and three CRD groups randomly, 6 rats in each group. Two groups of CRD rats were treated with MT (cat. no. M5250; MilliporeSigma) administered intraperitoneally with the dosages of 5 and 10 mg/kg/d, as the low dosage group (CRD + MT-LD) and high dosage group (CRD + MT-HD), while the other groups were treated with vehicle (equivalent volume of normal saline). To explore the association between CRD and erectile function, a CRD model was constructed by altering daily light-dark cycles in rats (24-26). Rats were housed under a 12/12-h light/dark cycle (LD 12:12, lights on at Zeitgeber time (ZT) 0 and lights off at ZT12). The lights for CRD group were switched to LD 2:2 for 4 weeks, the light source was a white, fluorescent lamp (500 lux at cage level), and then weekly body weight monitoring was conducted.

MT administration protocol and solution preparation: MT (MilliporeSigma) was administered intraperitoneally (i.p.) once daily for 4 consecutive weeks, starting from the first day of the CRD modeling protocol. To maintain consistency with the circadian rhythm experiment, MT was injected at a fixed Zeitgeber time (ZT1), i.e., 1 h after lights on (9:00 AM under a 12:12 light-dark cycle). The temporal relationship between MT injection and CRD modeling was as follows: each day, the light cycle was first changed to the CRD schedule (LD 2:2), and MT was administered intraperitoneally within 30 min thereafter. MT is a lipophilic compound with poor solubility in aqueous vehicles. Therefore, a stock solution was first prepared by dissolving 100 mg MT in 4.305 ml dimethyl sulfoxide (DMSO) to obtain a 100 mM stock solution. The stock solution was aliquoted into amber tubes and stored at -20˚C protected from light. On each day of administration, the stock solution

was freshly diluted with sterile normal saline (0.9% NaCl) to achieve the desired working concentrations (5 mg/kg for low dose, 10 mg/kg for high dose). The final concentration of DMSO in the working solution was ≤0.1% (v/v), a concentration previously shown to have no adverse effects on animal physiology or erectile function. The solution was vortexed and, if necessary, briefly sonicated to ensure complete dissolution before injection. Control animals received an equivalent volume of vehicle (sterile normal saline containing 0.1% DMSO).

Cell experimental design. The immortalized human umbilical vein endothelial cell line HUVEC-SV40 (SUNNCELL; https://www.app17.com/c163183/products/b3383_p1.html) was used in the present study. HUVECs were maintained in RPMI-1640 medium supplemented with 10% fetal bovine serum (both from Gibco; Thermo Fisher Scientific, Inc.) and 1% penicillin/streptomycin at 37˚C under 5% CO_2. To assess dose and time-dependent effects of MT and LPS, HUVECs were seeded in 96-well plates at $1x10^4$ cells/well and cultured for 24 h. Cells were then treated with specified concentrations of MT or LPS. Post-incubation, cell viability was measured using a Cell Counting Kit-8 (CCK-8) kit (cat. no. AR1160; Wuhan Boster Biological Technology, Ltd.) according to the manufacturer's protocol. Briefly, 10 μl of CCK-8 solution was added to each well containing 100 μl of culture medium. The plates were then incubated at 37˚C for 2 h in a humidified incubator with 5% CO_2. Absorbance was quantified at 450 nm using a Multiskan FC microplate reader (Thermo Fisher Scientific, Inc.). HUVECs were categorized into seven distinct experimental groups as follows: Control, LPS (1 mg/l), LPS + MT (800 μM), LPS + MT + ML385 (20 μM), LPS + MCC950 (20 μM), LPS + MT + BMS986299 (20 μM), and LPS + NAC (10 mM).

Evaluation of erectile function. Erectile function was measured from 10:00 to 12:00 a.m, and the penile tissue was subsequently dissected. Moreover, erectile function was assessed by recording the maximum intracavernous pressure (mICP) and mICP/mean arterial pressure (MAP) ratio as previously described (27). Rats were anesthetized by intraperitoneal injection of 3% pentobarbital sodium (30 mg/kg), the carotid was carefully exposed and cannulated with a heparinized detaining venipuncture (26 G) needle to monitor the arterial pressure through a pressure transducer. The cavernous nerve (CN) was carefully separated with a low midline abdominal incision, then a heparinized scalp acupuncture needle was inserted into the penile crus to record ICP through another pressure transducer. When the CN was electrically stimulated (using a voltage of 5 V at frequency of 20 Hz, pulse width of 5 msec, and sustained for 60 sec) (27), the ICP and arterial pressure were simultaneously recorded using a BL420 bio-function experiment system (Chengdu TME Technology Co., Ltd.). The mICP and MAP were analyzed, and the final mICP/MAP ratio and total ICP (area under curve, AUC-ICP) were calculated. At the end of the experiment, all rats were euthanized by intraperitoneal injection of excessive pentobarbital sodium (150 mg/kg), and death was confirmed by cardiac arrest, respiratory arrest and corneal reflex loss.

RNA-sequencing (RNA-seq) and bioinformatics analysis. Penile corpus cavernosum tissues were obtained from rats in the Control, CRD, and CRD + MT-HD groups. Total RNA was isolated with TRIzol reagent (Invitrogen; Thermo Fisher Scientific, Inc.). Total RNA was extracted, and sequencing libraries were prepared using TruSeq Stranded mRNA Library Prep Kit. The concentration of the final libraries was measured using a Qubit 4.0 Fluorometer with the Qubit dsDNA HS Assay Kit, and the fragment size distribution was assessed using an Agilent 2100 Bioanalyzer with the High Sensitivity DNA Kit. Each library was loaded at a final concentration of 10 nM onto the Illumina NovaSeq 6000 platform (Illumina, Inc.) according to the manufacturer's instructions for paired-end sequencing (2x150 bp). Sufficient double-stranded complementary DNA (dsDNA) for library preparation was generated through SMART pre-amplification (cat. no. 634925/634926; Takara Bio USA, Inc.). The dsDNA was then fragmented using dsDNA fragmentase, and fragments of the desired size were selected with sample purification beads. The resulting ligation product was amplified by PCR to construct the sequencing library. Raw reads obtained from sequencing included adapter sequences and low-quality bases. These were filtered using Cutadapt (version: cutadapt-1.9) (28) to generate high-quality clean reads. The clean data were then aligned to the rat reference genome for gene expression quantification and subsequent bioinformatic analyses.

Molecular docking and molecular dynamics simulations. The predicted protein structures were generated using AlphaFold (https://deepmind.google/technologies/alphafold/). Both structures were subsequently prepared with AutoDockTools-1.5.7 (https://autodock.scripps.edu), including manual removal of water molecules, addition of hydrogens, and other structural refinements. Protein-protein docking was then carried out using the GRAMM web server (29-31). The resulting complex was further optimized in AutoDockTools-1.5.7. Finally, protein-protein interaction (PPI) analysis and visualization were performed using PyMOL (pymol.org).

Masson trichrome staining. Penile corpus cavernosum was fixed in 4% paraformaldehyde, paraffin-embedded, and sectioned at 5 μm. Histological analysis included Masson trichrome staining per standard protocols. Smooth muscle and collagen content in penile corpus cavernosum were assessed by calculating their area ratio using Image-Pro Plus software (ver. 6.0; Media Cybernetics, Inc.).

Immunofluorescence (IF) staining. The paraffin-embedded sections of penile corpus cavernosum tissues and HUVECs slides were used for IF to explore the expression of target proteins. The primary antibodies used for incubating sections overnight at 4˚C were rabbit anti-eNOS (1:100; cat. no. AF0096; Affinity Biosciences), anti-Nrf2 (1:200; cat. no. 33123-1-AP; Proteintech Group, Inc.), anti-HO-1 (1:100; cat. no. 10701-1-AP; Proteintech Group, Inc.), anti-α-SMA (1:100; cat. no. 14395-1-AP; Proteintech Group, Inc.) and anti-NLRP3 (1:100; cat. no. DF7438; Affinity Biosciences). Then, appropriate secondary antibodies [Alexa Fluor 488-conjugated goat anti-rabbit IgG (H+L); 1:200; cat. no. A32731; Invitrogen; Thermo Fisher Scientific, Inc.] were selected for further incubation. A total of five random fields per group were imaged. Semi-quantitative analysis of relative fluorescence intensity was conducted using Image-Pro Plus software (v6.0).

Terminal deoxynucleotidyl transferase dUTP nick end labeling (TUNEL) staining for pyroptosis detection. To detect pyroptotic cells, TUNEL staining was performed using a commercial kit according to the manufacturer's instructions, with modifications for paraffin-embedded sections. Briefly, penile corpus cavernosum tissue sections were dewaxed and rehydrated. After washing with PBS (three times, 5 min each), sections were incubated with proteinase K working solution (1 μl of 100X proteinase K in 99 μl PBS) for 20 min at 37˚C to permeabilize the tissue. Following three additional PBS washes, sections were incubated with TdT equilibration buffer for 20 min at 37˚C. The buffer was then removed, and labeling working solution (35 μl TdT equilibration buffer+10 μl labeling solution + 5 μl TdT enzyme) was added to each section. Sections were incubated in a humidified chamber for 60 min at 37˚C in the dark. After three PBS washes, nuclei were counterstained with DAPI working solution [4 μl DAPI reagent (25 μg/ml) in 96 μl PBS] for 5 min at room temperature in the dark. Sections were washed four times with PBS, mounted with anti-fade mounting medium, and immediately observed under a fluorescence microscope.

Double IF for Caspase-1 and TUNEL. For simultaneous detection of Caspase-1 and TUNEL, sections were first processed for TUNEL staining as aforementioned, followed by IF staining for Caspase-1 using rabbit anti-Caspase-1 primary antibody (1:100; cat. no. 31020-1-AP; Proteintech Group, Inc.) and appropriate Alexa Fluor-conjugated secondary antibody. Nuclei were counterstained with DAPI. Co-localization of Caspase-1 and TUNEL signals was assessed to identify pyroptotic cells (18,32). The percentage of Caspase-1$^+$/TUNEL$^+$ double-positive cells was calculated from at least five random fields per section.

Immunohistochemistry (IHC) staining. The paraffin-embedded sections of penile corpus cavernosum tissues were fixed in 4% paraformaldehyde at 4˚C for 24 h, embedded in paraffin, and cut into sections as aforementioned. Sections were incubated with rabbit anti-eNOS (1:100; Affinity Biosciences), anti-Nrf2 (1:200; Proteintech Group, Inc.), anti-HO-1 (1:100; Proteintech Group, Inc.), anti-Collagen-I (1:200; Abcam) and anti-Collagen-III (1:200; Abcam) overnight at 4˚C. Then the sections were washed by PBS and incubated by relevant HRP-conjugated goat anti-rabbit IgG (H+L) secondary antibodies (1:500; cat. no. 31460; Thermo Fisher Scientific, Inc.) for 1 h at room temperature. Five random fields per group were imaged. Semi-quantitative analysis of relative fluorescence intensity was conducted using Image-Pro Plus software (v6.0).

Scanning electron microscope (SEM). Fresh penile corpus cavernosum tissues were dissected into ≤1 mm^3 fragments and fixed in 2.5% glutaraldehyde for 4 h. Samples were post-fixed in 1% osmium tetroxide for 2 h at room temperature. After dehydration through a graded ethanol series and transition in propylene oxide, tissues were embedded in resin and sectioned into 60-80 nm ultrathin slices. Sections were dual-stained with uranyl acetate and lead citrate, then observed and imaged using a SEM.

Measurement of NO and cGMP levels. NO and cGMP levels were quantified in fresh penile corpus cavernosum tissues and HUVECs. NO Assay Kit (cat. no. A013-2-1; Nanjing Jiancheng Bioengineering Research Institute) was applied to detect the level of NO. cGMP ELISA Kit (cat. no. JM-01434R2; JINGMEI; http://jsjmsw.com/) was used to measure the concentration of cGMP. They were performed according to the manufacturer's protocols. The levels of NO and cGMP were normalized to the protein concentration.

Reverse transcription-quantitative PCR (RT-qPCR) analysis. Total RNA was extracted from rat penile corpus cavernosum tissues and HUVECs using a Rapid RNA Isolation Kit (cat. no. G3013; Wuhan Servicebio Technology Co., Ltd.). cDNA was synthesized with a PrimeScript™ RT Reagent Kit (cat. no. RR047A; Takara Bio, Inc.) according to the manufacturer's instructions. RT-qPCR was performed on a CFX96 Real-Time System (Bio-Rad Laboratories, Inc.) using TB Green Premix Ex Taq II (cat. no. RR820A; Takara Bio, Inc.). The thermocycling conditions were as follows: Initial denaturation at 95˚C for 30 sec, followed by 40 cycles of denaturation at 95˚C for 5 sec and annealing/extension at 60˚C for 30 sec. A melting curve analysis was performed after amplification to verify the specificity of the PCR products (95˚C for 15 sec, 60˚C for 1 min, then gradually increasing to 95˚C). The relative expression levels of target genes were calculated using the $2^{-\Delta\Delta Cq}$ method (33), where ΔCt=Ct(target)-Ct(GAPDH) and $\Delta\Delta$Ct=ΔCt(treatment)-ΔCt(control). The specific primers used in RT-qPCR are shown in Tables SI and SII.

Western blotting. Penile corpus cavernosum tissues and HUVECs were lysed in RIPA buffer (cat. no. R0010; Beijing Solarbio Science & Technology Co., Ltd.) containing protease inhibitor cocktail (cat. no. HY-K0010; MedChemExpress), followed by sonication and centrifugation (12,000 x g, 15 min, 4˚C) to collect supernatants. Total protein concentration was determined by BCA assay (cat. no. AR0146; Boster Biological Technology). Protein samples (30 μg) were separated by 10% SDS-PAGE and transferred to PVDF membranes. Membranes were blocked with 5% BSA (http://www.genenode.com)/TBST (0.1% Tween-20) for 1 h at room temperature, then incubated overnight at 4˚C with primary antibodies: Rabbit anti-Nrf2 (1:2,000) and anti-HO-1 (1:1,000). After primary incubation, membranes were probed with species-matched HRP-conjugated secondary antibodies (1:5,000) for 1 h at room temperature. Band intensities were quantified using ImageJ software (version 1.53t; National Institutes of Health) and normalized to GAPDH.

Analysis of ROS and mitochondrial ROS. Cellular ROS and mitochondrial ROS (mtROS) levels were assessed using the fluorescent probes H2DCFH-DA (cat. no. D6470; Beijing Solarbio Science & Technology Co., Ltd.) and MitoSOX™ Red Mitochondrial Superoxide Indicator (cat. no. HY-D1055; MedChemExpress), respectively.

For tissue sample preparation, penile corpus cavernosum tissue fragments were enzymatically digested at 37˚C for 30 min, filtered through a 70-μm nylon mesh, and centrifuged at 500 x g. The pellet was washed twice with PBS and subsequently incubated with 10 μM H2DCFH-DA at 37˚C for 1 h.

After incubation, the samples were centrifuged at 1,000 x g and washed again twice with PBS. Fluorescence intensity was measured using a microplate reader at Ex/Em=488/525 nm.

For the cell-based assay, HUVECs cultured on adherent slides were incubated with 10 μM H2DCFH-DA at 37˚C for 30 min under light-protected conditions, following the manufacturer's instructions. Fluorescence images were acquired immediately using a fluorescence microscope, with five random fields captured per sample. Semi-quantitative analysis of fluorescence intensity was performed using Image-Pro Plus software (v6.0). For mtROS detection, the MitoSOX™ Red probe was used according to the manufacturer's protocol, and fluorescence was detected at Ex/Em=510/580 nm under light-protected microscopy.

Detection of malondialdehyde (MDA), reduced glutathione (GSH), SOD and total antioxidant capacity (T-AOC) levels. MDA, GSH, SOD and T-AOC levels were quantified in rat CC tissue homogenates and HUVECs lysates using commercial kits: MDA (cat. no. BC0025), GSH (cat. no. BC1175), SOD (cat. no. BC5165) and T-AOC (cat. no. BC1315; all from Beijing Solarbio Science & Technology Co., Ltd.). Assays were performed strictly according to manufacturer's protocols. All values were normalized to total protein concentration.

Detection of mitochondrial membrane potential (MMP). MMP was assessed using JC-1 staining (cat. no. E-CK-A301; Elabscience Biotechnology, Inc.) and analyzed via fluorescence microscopy.

Statistical analysis. All results were presented as mean ± standard deviation and analyzed with GraphPad Prism software (version 9.5.0; Dotmatics). Shapiro-Wilk test was used for normality and Levene's test was used for homogeneity of variance before applying parametric tests. For data that did not meet normality or equal variance assumptions, Kruskal-Wallis H test followed by Dunnett's multiple comparisons test was utilized. It was clarified that Dunnett's test was used for comparisons against the control group (primary aim), while Tukey's or Dunnett's tests were applied for all pairwise comparisons or non-parametric data, respectively. $P<0.05$ was considered to indicate a statistically significant difference. The number of independent biological replicates were as follows: n=6 per group for animal experiments; n=3 independent culture batches for cell experiments, each with technical triplicates.

Results

MT protects CRD-induced ED and preserves eNOS-NO-cGMP pathway in penile corpus cavernosum and HUVECs. As was shown, the CRD group (44.91±7.51 mmHg) showed significantly lower mICP than Control group (76.82±3.81 mmHg, $P<0.0001$); however, the CRD + MT-LD (57.03±2.03 mmHg, $P=0.0008$) and CRD + MT-HD (66.15±2.49 mmHg, $P<0.0001$) groups significantly increased mICP than the CRD group (Fig. 1A and C); the total ICP also showed a similar trend (Fig. 1A and D). Meanwhile, the CRD group significantly reduced mICP/MAP ratio (0.38±0.07) than Control group (0.64±0.03, $P<0.0001$), while the CRD + MT-LD (0.50±0.02, $P=0.0013$) and CRD + MT-HD (0.59±0.05, $P<0.0001$) significantly increased it (Fig. 1A and F). Moreover, the bICP and MAP were consistent among the four groups ($P>0.05$) (Fig. 1A, B and E). These results suggested that CRD impaired rats' normal erectile function, while MT demonstrated a protective effect for CRD-induced ED. In addition, these procedures had no impact on rats' mean body weight ($P>0.05$) (Fig. S1), which excluded potential confounding such as systemic metabolic effects.

The IF and IHC staining of penile corpus cavernosum revealed that CRD significantly reduced eNOS expression, which was partially preserved by MT-LD and MT-HD (Fig. 1G-J). Meanwhile, the penile corpus cavernosum of CRD group also demonstrated significantly decreased NO and cGMP concentrations, which was also inhibited by MT-LD and MT-HD (Fig. 1K and L). These *in vivo* results also suggested that MT could preserve the CRD-induced ED.

To further confirm these findings, LPS-treated HUVECs were selected to imitate CRD stimulation *in vitro* (34,35) to verify the underlying mechanism, while the specific concentrations and exposure times of LPS and MT for HUVECs were provided in the following statement. Firstly, HUVECs were treated with different concentrations of LPS and MT for different time intervals to evaluate their cytotoxicity. It was found that the concentration of LPS up to 0.5 mg/l and MT up to 1,600 μM had significant effects on the viability of HUVECs for 24 h (Fig. S3A and C). However, LPS with 1.0 mg/l for 24 h reduced HUVECs viability to 52.03% than the control group, indicating a cytotoxic effect with an approximate IC_{50} of 1.0 mg/l, whereas MT with 800 μM was well-tolerated with no significant effect on viability even after 48 h (Fig. S3B and D). Thus, HUVECs treated with LPS at 1.0 mg/l were used to establish a CRD stimulation model *in vivo*. Therefore, cells were incubated with 400 or 800 μM MT for 2 h before exposure to 1.0 mg/l LPS. The protective effect of 800 μM MT was significantly more pronounced, a finding consistently corroborated by both CCK-8 and phase-contrast microscopy assay (Fig. S3E and F). As was shown, LPS could significantly reduce eNOS expression while decreased NO and cGMP levels, confirming that CRD could impair HUVECs; however, these damages were reversed by MT (Fig. 1M-P).

Collectively, these *in vivo* and *in vitro* results suggested that CRD impaired rats' erectile function and injured HUVECs by disrupting eNOS-NO-cGMP pathway, however, MT treatment could reduce these alterations to ameliorate CRD-induced ED.

Verification of CRD model establishment at the molecular level. To confirm that photoperiodic manipulation successfully induced circadian rhythm disorders, the expression of core clock genes was first analyzed in the corpus cavernosum tissue of a model rat by sequencing data. As revealed in Fig. S4, firstly, RNA quality was evaluated using the Affy package in R software (version 4.2.1; https://www.R-project.org) and gene expression levels were normalized using limma package (https://bioconductor.org/packages/limma/) and StringTie software. (https://github.com/gpertea/stringtie). Visual analysis was conducted using a box plot of relative logarithmic expression levels, and the results demonstrated favorable consistency among samples within each group (Fig. S4A). Secondly, the

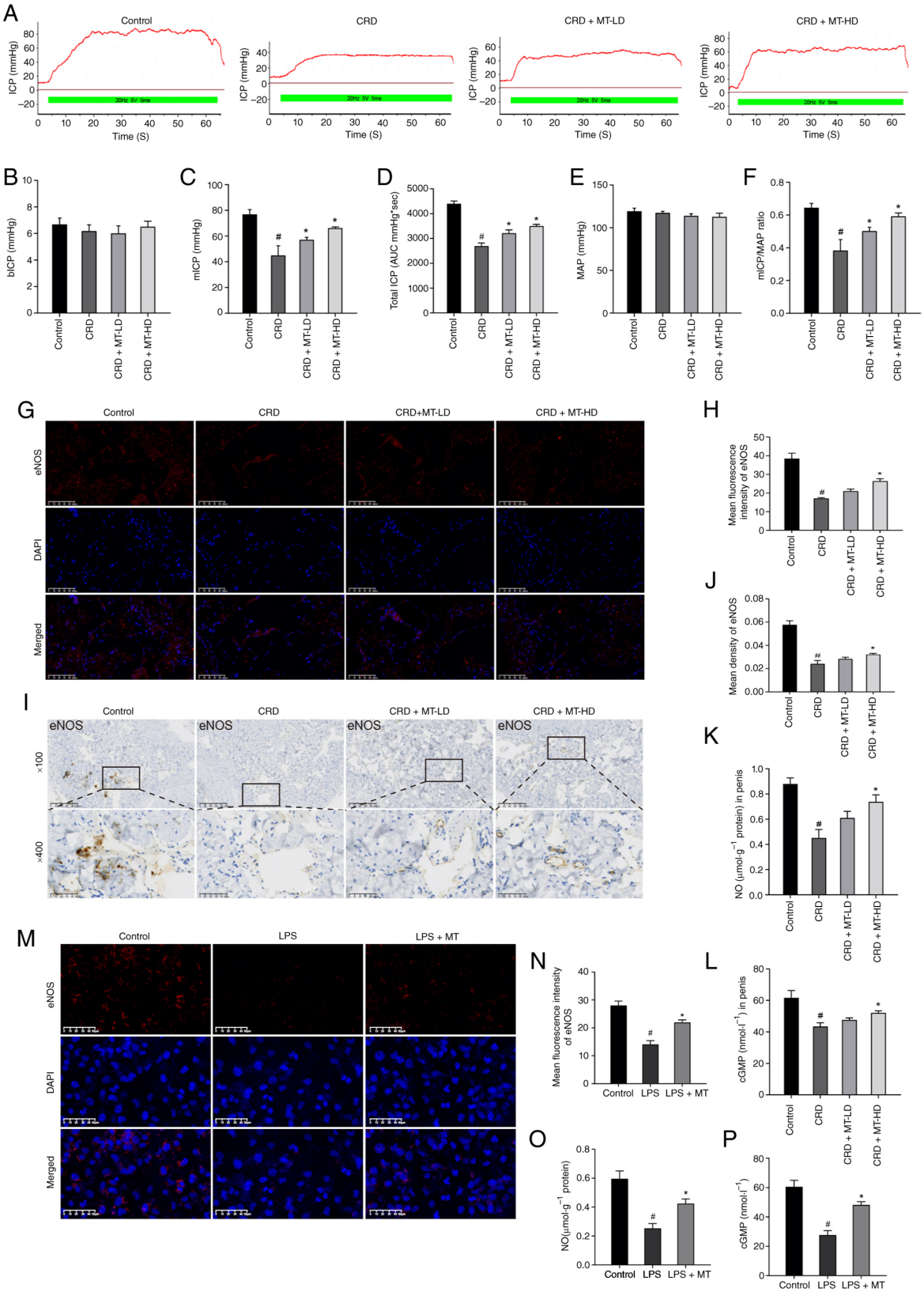

Figure 1. MT protects CRD-induced ED and preserves eNOS-NO-cGMP pathway in penile corpus cavernosum and HUVECs. (A) Representative ICP with the electrical stimulation of the CN. (B-F) The erectile function was evaluated by (B) bICP, (C) mICP, (D) Total ICP (represented by area under the curve), (E) MAP and (F) mICP/MAP. (G and I) Representative images of immunofluorescence staining and IHC staining for eNOS in penile corpus cavernosum, respectively. (H and J) Semi-quantitative data of eNOS expression as relative fluorescence intensity and density in penile corpus cavernosum, respectively. There were three replicates in this experiment (n=3). (K and L) NO content and cGMP content in penile corpus cavernosum, respectively. (M) Representative images of IHC staining for eNOS in HUVECs. (N) Semi-quantitative data of eNOS expression as relative fluorescence intensity in HUVECs. (O and P) NO content and cGMP content in HUVECs, respectively. $^{\#}$P<0.05 compared with the control group; *P<0.05 compared with the CRD or LPS group. MT, melatonin; CRD, circadian rhythm disruption; ED, erectile dysfunction; eNOS, endothelial nitric oxide synthase; NO, nitric oxide; cGMP, cyclic guanosine monophosphate; HUVECs, human umbilical vein endothelial cells; ICP, intracavernous pressure; CN, cavernous nerve; mICP, maximal ICP; MAP, mean arterial pressure; IHC, immunohistochemistry; LD, low dosage; HD, high dosage.

limma package and Wilcoxon test were used to screen differentially expressed genes (DEGs), with a screening threshold set at |logFC|>0.5 and FDR<0.05. The results showed that a total of 872 DEGs were identified between the Control group and the CRD group, of which 389 genes were significantly downregulated, and 483 genes were significantly upregulated (Fig. S4B). Further differential expression analysis was conducted on the core clock genes in the selected DEGs. The heatmap results identified that 12 core clock genes, including Per1/2/3, Npas2, Csnk1e, Cry1/2, Nr1d1/2, Clock, Rorα and Timeless, were generally upregulated in the CRD group, indicating the successful construction of a CRD model by changing the light cycle (Fig. S4C). Secondly, through IF, IHC, WB and RT-qPCR experiments, it was found that compared with the control group, the protein and mRNA expression levels of the core circadian clock gene Per1 in the corpus cavernosum tissue of CRD group rats were significantly increased (Fig. S5A-G). This result is consistent with RNA-seq data, and a CRD model was successfully established at the functional and molecular levels.

Rationale for using LPS-induced HUVECs to mimic CRD in vitro. Haspel *et al* (34) demonstrated that LPS exposure *in vitro* and *in vivo* leads to reprogramming of the circadian clock, including changes in the expression of core clock genes such as Per1, Per2 and Bmal1. Ryzhikov *et al* (35) further demonstrated that LPS induces a CRD-like state in cultured cells, characterized by loss of rhythmic expression of clock control genes. In the authors' preliminary experiments, LPS treatment significantly upregulated the expression of Per1 in HUVECs (Fig. S6), simulating the molecular clock disruption observed in the corpus cavernosum of rats with CRD. This validates the use of LPS treated HUVEC as a relevant *in vitro* model for studying the mechanism of CRD-induced endothelial injury.

MT reduces microstructural damage of penile corpus cavernosum. For the microstructural changes of penile corpus cavernosum, Masson trichrome staining showed that SMC/Collagen ratio in CRD group was significantly reduced, which was increased in CRD + MT-LD and CRD + MT-HD groups (Fig. 2A and B). IF staining revealed that the reduced α-SMA in CRD group was ameliorated in CRD + MT-LD and CRD + MT-HD groups (Fig. 2C and D), while IHC staining presented that CRD + MT-LD and CRD + MT-HD significantly attenuated Collagen-I and III deposition than CRD group (Fig. 2E-H). For the SEM of penile corpus cavernosum, CRD group presented that collagen fibers (→) in the outer layers of tunica albuginea were irregularly lined and sinusoidal (S) spaces were significantly narrowed; however, these collagen fibers (→) were regularly lined and sinusoidal (S) spaces were widened in CRD + MT-HD group (Fig. 2I and J). All these demonstrated that CRD impaired the microstructural integrity of penile corpus cavernosum, which were partially reversed through MT intervention.

Oxidative stress is a core pathway in the treatment of ED with MT. To elucidate the therapeutic mechanisms of MT on CRD-induced ED, a systematic bioinformatics analysis was performed. Firstly, bioinformatic screening across multiple databases [including GeneCards (https://www.genecards.org), STRING (https://string-db.org), DAVID, PubChem (https://pubchem.ncbi.nlm.nih.gov), CTD (https://ctdbase.org) and OMIM (https://www.omim.org)] identified 1,500 ED-associated genes and 825 predicted MT target genes, with 284 overlapping targets selected for further analysis (Fig. 3A). PPI network construction and analysis of these overlapping targets (Fig. 3B and C) identified 63 core targets (Fig. 3D), which notably included oxidative stress-related genes (OSRGs). These findings establish oxidative stress as a core pathway through which MT exerts its therapeutic effects in ED.

The oxidative stress level of rats' penile corpus cavernosum was thus evaluated. The oxidative stress markers (ROS and MDA) in CRD group were significantly increased and antioxidant parameters (GSH, SOD and T-AOC) were decreased, all of which were partially reversed by MT-LD and MT-HD (Fig. 3E-I). All these inferred that oxidative imbalance is an essential pathological process for CRD-induced ED, which is also a core therapeutical mechanism for MT.

MT inhibits oxidative stress via Nrf2/HO-1 pathway in penile corpus cavernosum and HUVECs. Sequencing for penile corpus cavernosum was further performed, which identified 1,320 DEGs between CRD and CRD + MT-HD groups (Fig. 4A); all the top 20 OSRGs exhibited significantly differential expression. Notably, the core Nrf2 and HO-1 of OSRGs in CRD + MT-HD group were significantly upregulated compared with CRD group (Fig. 4B), suggesting their crucial role in mediating the therapeutic effect of MT. To further investigate whether MT directly interacts with Nrf2 and HO-1, molecular docking was performed. The results showed binding energies of -5.7 kcal/mol for Nrf2 and -6.4 kcal/mol for HO-1, indicating stable binding between MT and both proteins (Fig. 4C and D). Given the core role of Nrf2 (36) and HO-1 (37) in oxidative stress response, it was hypothesized that MT primarily exerted antioxidant effects through activating Nrf2/HO-1 pathway.

In vivo analyses (IF and IHC of penile corpus cavernosum) revealed that Nrf2 and HO-1 protein expression levels were slightly increased in CRD rats, whereas MT intervention significantly upregulated their levels (Fig. 4E-L); this pattern was corroborated in BCNI rat model, that the disease itself did not alter Nrf2 or HO-1 expression, yet antioxidant treatment elevated them (38). To validate these findings, the LPS-treated HUVECs were selected to imitate CRD stimulation *in vitro* (34,35). Consistent with the *in vivo* data, western blotting and RT-qPCR analysis demonstrated that the levels of Nrf2 and HO-1 in the LPS + MT group were significantly higher than LPS group, while Nrf2 inhibitor (ML385) significantly reduced Nrf2 and HO-1 expression compared with LPS + MT group (Fig. 4M-R).

It has been previously proved by the authors that oxidative stress was involved in the therapeutic effects of MT on CRD-induced ED; whether this occurs through Nrf2/HO-1 pathway remains unclear. The present *in vitro* experiments demonstrated that MT reduced the LPS-induced elevation of oxidative stress markers (ROS, mtROS and MDA) while rescued reduction of antioxidant parameters (MMP, GSH, SOD and T-AOC); notably, these beneficial effects were partially reversed by Nrf2 inhibitor (ML385), indicating that

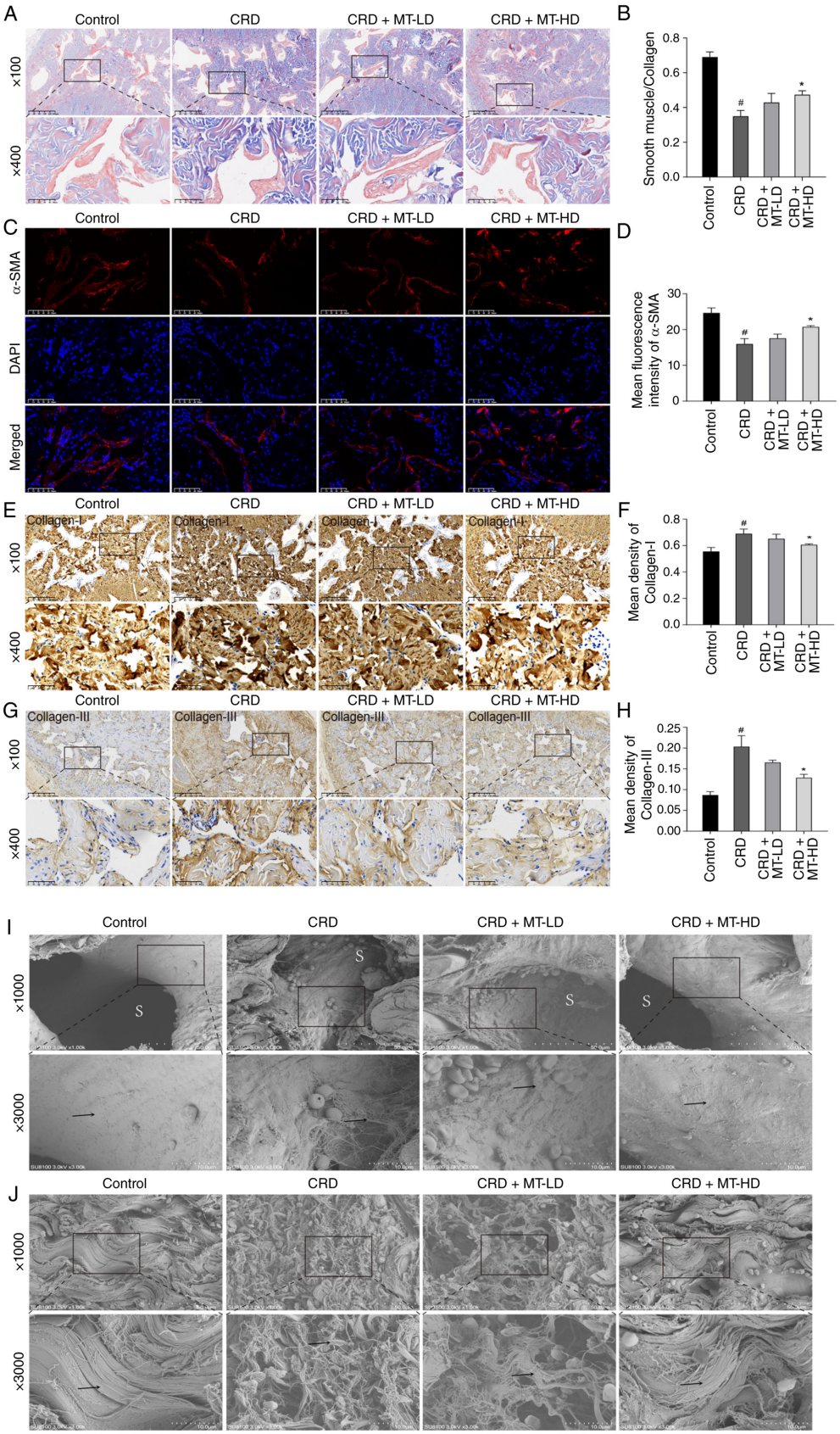

Figure 2. MT reduces the microstructural damage of the penile corpus cavernosum. (A) Representative images of Masson trichrome staining. Smooth muscle and collagen were stained red and blue in penile corpus cavernosum, respectively. (B) Semi-quantitative data of the ratio of smooth muscle and collagen in penile corpus cavernosum. (C) Representative images of immunofluorescence staining for α-SMA in penile corpus cavernosum. (D) Semi-quantitative data of α-SMA expression as relative fluorescence intensity in penile corpus cavernosum. (E and G) Representative images of immunohistochemistry staining for Collagen-I and Collagen-III in penile corpus cavernosum, respectively. (F and H) Semi-quantitative data of Collagen-I and Collagen-III expression as relative density in penile corpus cavernosum, respectively. (I and J) Alterations of the ultrastructure of the penile corpus cavernosum. There were three replicates in this experiment. $^{\#}$P<0.05 compared with the control group; *P<0.05 compared with the CRD group. MT, melatonin; α-SMA, alpha smooth muscle actin; CRD, circadian rhythm disruption; LD, low dosage; HD, high dosage.

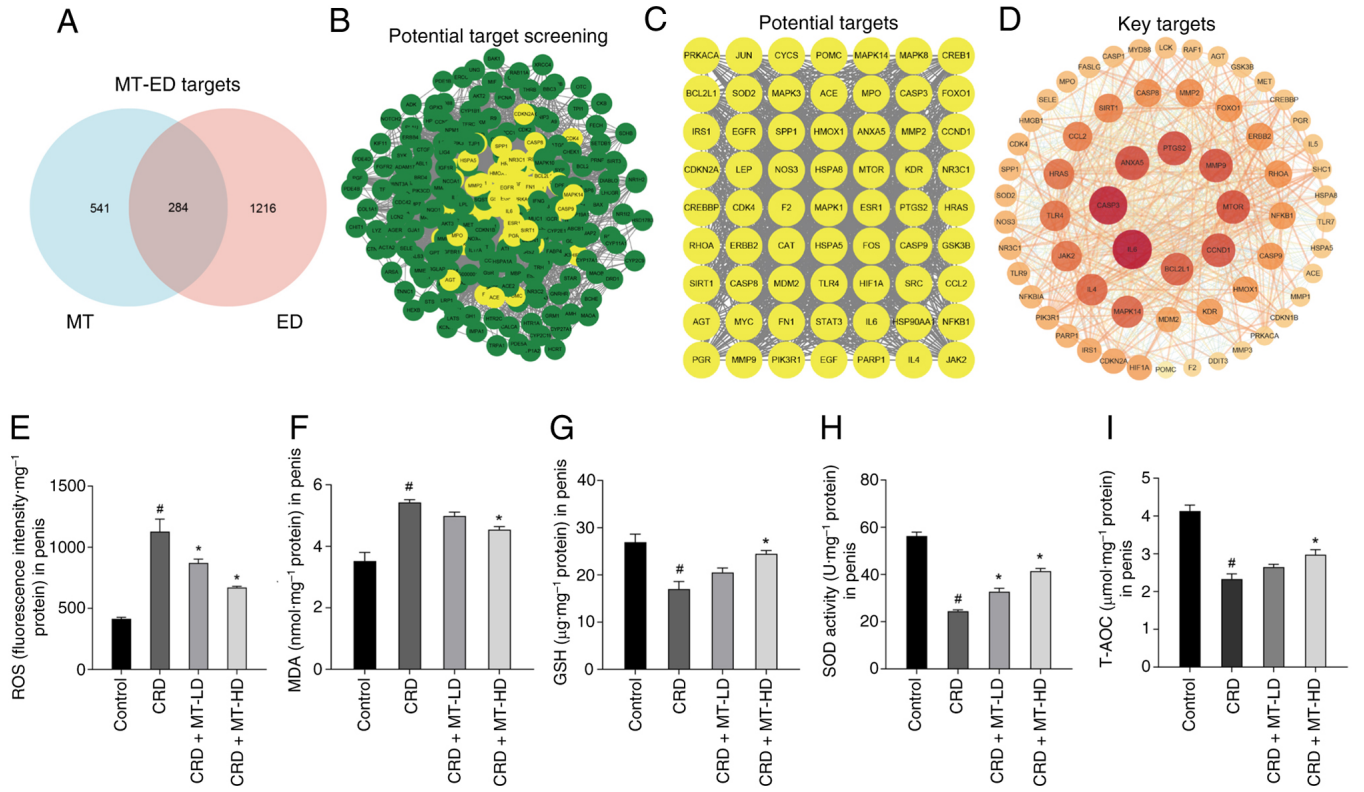

Figure 3. Oxidative stress is a core pathway in the treatment of ED with MT. (A) Overlapping targets between MT and ED. (B) Screening process of potential therapeutic targets. (C) Final set of candidate targets. (D) Core targets derived from protein-protein interaction network analysis. (E-I) Levels of ROS, MDA and GSH, as well as SOD activity and T-AOC, were measured in the penile corpus cavernosum of CRD rats, respectively. #P<0.05 compared with the control group; *P<0.05 compared with the CRD group. ED, erectile dysfunction; MT, melatonin; ROS, reactive oxygen species; MDA, malondialdehyde; GSH, reduced glutathione; SOD, superoxide dismutase; T-AOC, total antioxidant capacity; CRD, circadian rhythm disruption; LD, low dosage; HD, high dosage.

MT exerted antioxidant effects through activating Nrf2/HO-1 pathway (Fig. 5A-J).

MT suppresses NLRP3-mediated pyroptosis in penile corpus cavernosum and HUVECs. To further explore the downstream mechanism of how MT regulates CRD-induced ED through oxidative stress, sequencing analysis was subsequently performed on penile corpus cavernosum tissues from CRD rat model groups. A total of 37 pyroptosis-related DEGs were identified by intersecting RNA-seq data from CRD and CRD + MT-HD groups with pyroptosis-related genes from GeneCard (Fig. 6A). PPI network analysis was constructed using STRING and visualized in Cytoscape (version 3.10.3; https://web.cytoscape.org). Functional enrichment analysis (DAVID; https://davidbioinformatics.nih.gov) showed significant involvement of the 'NOD-like receptor signaling pathway' (Fig. 6B). Based on these findings, along with the established link between NLRP3 and pyroptosis (39) (Fig. 6C), it was therefore hypothesized that NLRP3-mediated pyroptosis may contribute to the development of CRD-induced ED.

The IF staining of penile corpus cavernosum was performed to evaluate the core protein of pyroptosis (NLRP3, Caspase-1 and GSDMD). As was demonstrated, NLRP3 protein expression in rats with CRD was significantly increased, which was markedly attenuated following CRD + MT-LD and CRD + MT-HD groups (Fig. 6D and E). Meanwhile, both the caspase-1$^+$/TUNEL$^+$ index [identified as pyroptosis (18,32)] (Fig. 6F and G) and GSDMD expression (Fig. 6H and I) revealed consistent alterations of NLRP3, rising under CRD and declining after MT. The *in vitro* LPS-treated HUVECs also presented similar consequences. LPS significantly elevated the key pyroptosis protein levels (NLRP3, caspase-1 and GSDMD); however, all these alterations were partially reversed by MT treatment (Fig. 6J-O). These demonstrated that CRD promoted pyroptosis, whereas MT treatment alleviated this process.

To further elucidate the mechanism by which MT mitigates LPS-induced pyroptosis in HUVECs, a dual-intervention strategy was employed using the NLRP3 inhibitor (MCC950) and agonist (BMS986299). IF analysis demonstrated that both the NLRP3 inhibitor (MCC950) and MT similarly suppressed the LPS-induced upregulation of key pyroptosis markers (NLRP3, Caspase-1 and GSDMD). By contrast, the NLRP3 agonist (BMS986299) attenuated the inhibitory effect of MT on these LPS-induced pyroptosis markers (Fig. 6J-O). The present findings suggested that CRD could lead ED through inducing pyroptosis, whereas MT counteracted this effect through inhibiting NLRP3 activation.

MT alleviates NLRP3-mediated pyroptosis through suppression of oxidative stress. To further explore whether MT alleviates NLRP3-mediated pyroptosis through oxidative stress, we incorporated the Nrf2 inhibitor (ML385) and NLRP3 inhibitor/agonist (MCC950/BMS986299) to enable a systematic comparison across these targeted interventions. IF analysis revealed that MT significantly suppressed the LPS-induced up-regulation of pyroptosis markers, an

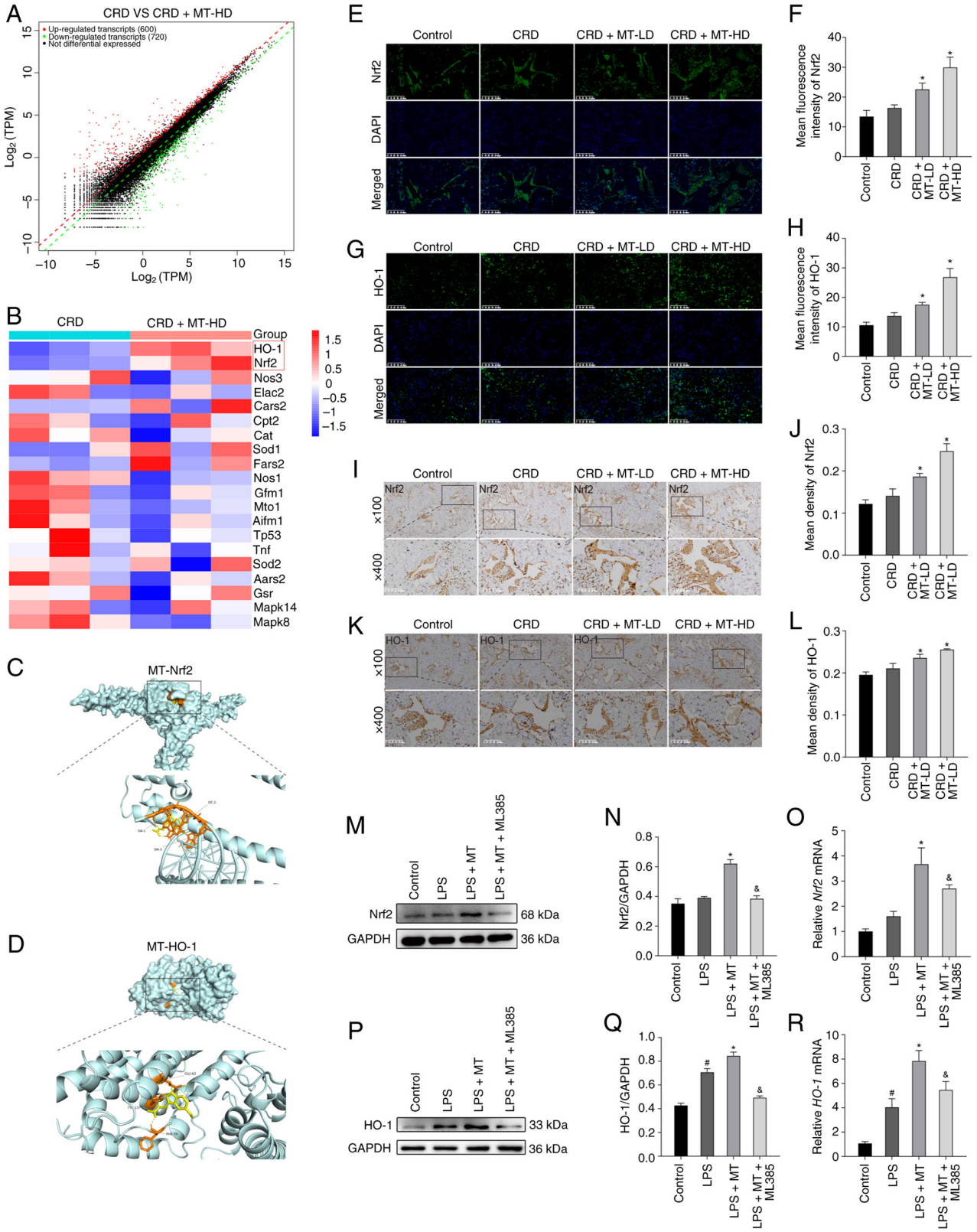

Figure 4. Identification of key targets and analysis of pathway effects in MT-mediated amelioration of ED. (A) Volcano plot showing the differentially expressed genes between the CRD and CRD + MT-HD groups. (B) Differential expression of oxidative stress-related genes in penile corpus cavernosum: a comparison between CRD and CRD + MT-HD groups. (C and D) Three-dimensional molecular docking of MT with Nrf2 and HO-1. (E and G) Representative images of immunofluorescence staining for Nrf2 and HO-1 in penile corpus cavernosum, respectively. (F and H) Semi-quantitative data of Nrf2 and HO-1 expression as relative fluorescence intensity in penile corpus cavernosum, respectively. (I and K) Representative images of immunohistochemistry staining for Nrf2 and HO-1 in penile corpus cavernosum, respectively. (J and L) Semi-quantitative data of Nrf2 and HO-1 expression as relative density in penile corpus cavernosum, respectively. (M and P) Representative western blot bands for Nrf2 and HO-1 in HUVECs, respectively. (N and Q) Semi-quantitative analysis of protein levels of Nrf2 and HO-1 in HUVECs, respectively. (O and R) Semi-quantitative analysis of mRNA levels of Nrf2 and HO-1 in HUVECs, respectively. There were three replicates in these experiments. $^{\#}$P<0.05 compared with the control group; *P<0.05 compared with the CRD or LPS group; $^{\&}$P<0.05 compared with the LPS + MT group. MT, melatonin; ED, erectile dysfunction; HD, high dosage; Nrf2, nuclear factor erythroid 2-related factor 2; HO-1, heme oxygenase 1; HUVECs, human umbilical vein endothelial cells; LPS, lipopolysaccharide; LD, low dosage.

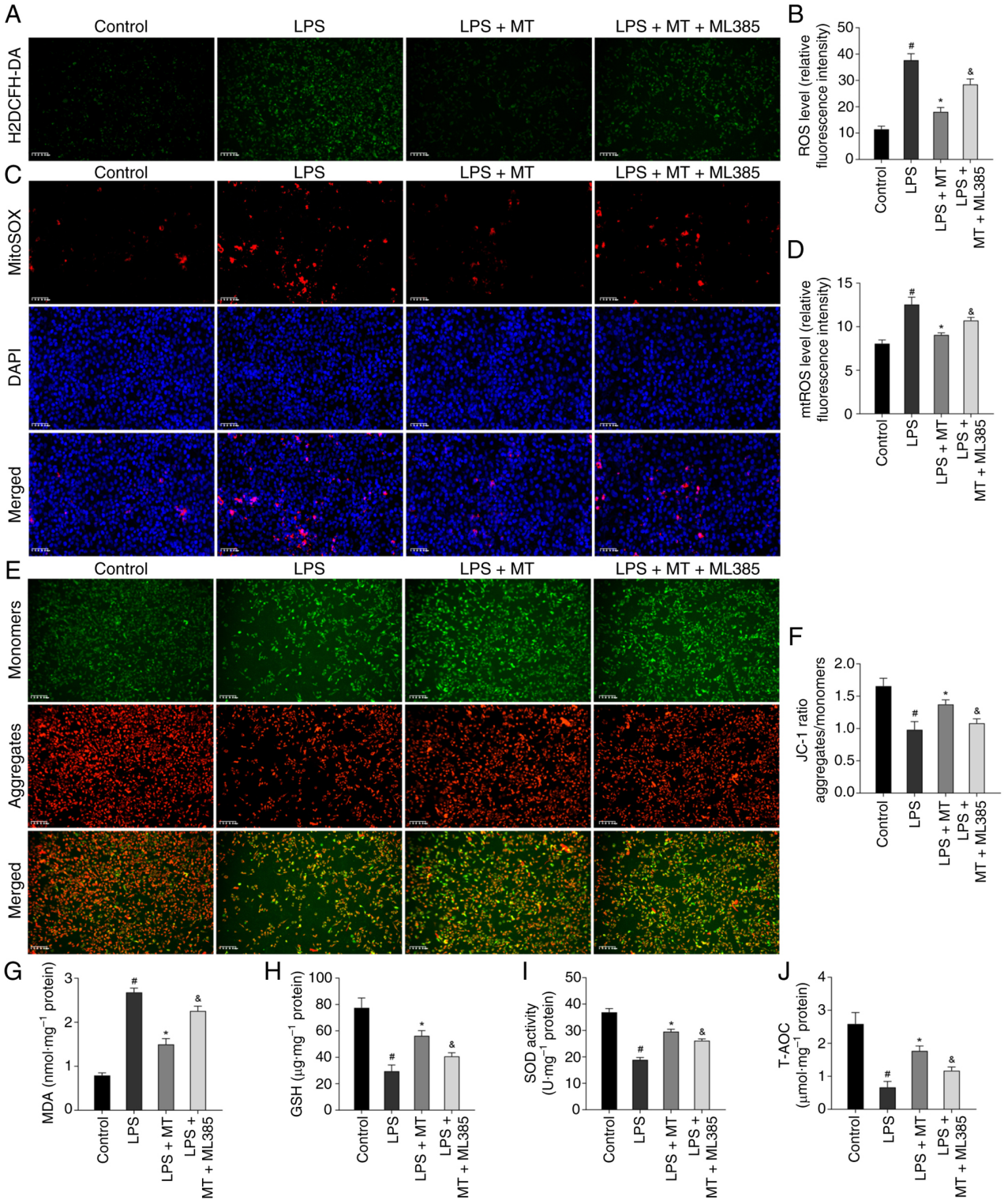

Figure 5. MT inhibits oxidative stress via Nrf2/HO-1 pathway in HUVECs. (A) Representative images of H2DCFH-DA staining for ROS in HUVECs. (B) Semi-quantitative data of ROS level as relative fluorescence intensity in HUVECs. (C) Representative images of MitoSOX Red staining for mtROS in HUVECs. (D) Semi-quantitative data of mtROS level as relative fluorescence intensity in HUVECs. (E) Representative images of JC-1 staining for MMP in HUVECs. (F) Semi-quantitative data of MMP as a relative JC-1 ratio in HUVECs. (G-J) Levels of MDA, GSH, as well as SOD activity and T-AOC were measured in HUVECs, respectively. #P<0.05 compared with the control group; *P<0.05 compared with the CRD or LPS group; &P<0.05 compared with the LPS + MT group. MT, melatonin; Nrf2, nuclear factor erythroid 2-related factor 2; HO-1, heme oxygenase 1; HUVECs, human umbilical vein endothelial cells; ROS, reactive oxygen species; mtROS, mitochondrial ROS; MMP, mitochondrial membrane potential; MDA, malondialdehyde; GSH, reduced glutathione; SOD, superoxide dismutase; T-AOC, total antioxidant capacity; LPS, lipopolysaccharide.

effect that was also found by NLRP3 inhibitor (MCC950). Meanwhile, Nrf2 inhibitor (ML385) completely abolished the protective effect of MT, an effect that was also found by NLRP3 agonist (BMS986299) (Fig. 6J-O). All these proved the core mechanism that MT alleviates NLRP3-mediated pyroptosis through suppression of oxidative stress.

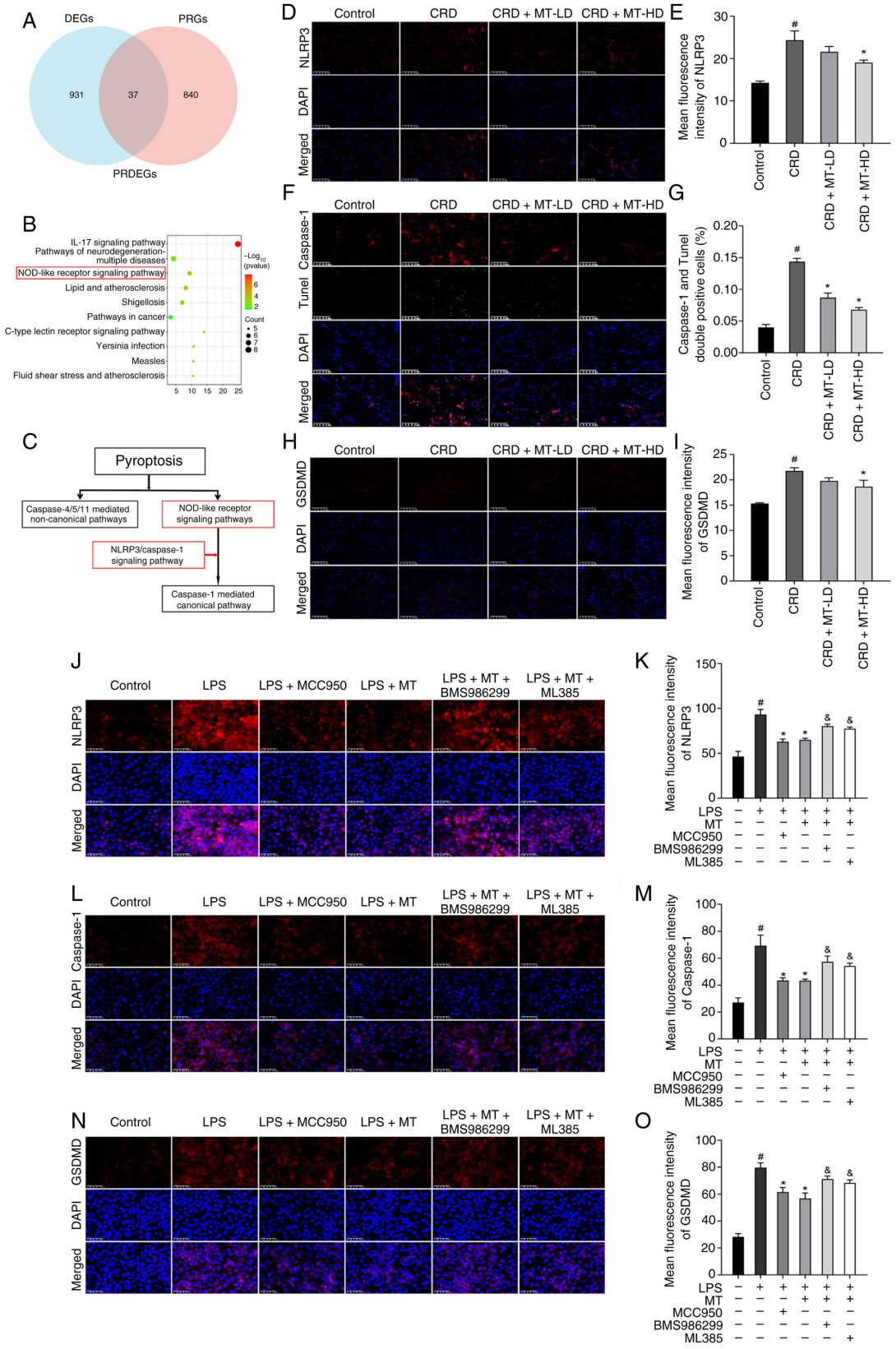

Figure 6. MT suppresses NLRP3-mediated pyroptosis in penile corpus cavernosum and HUVECs. (A) PRDEGs were identified from DEGs and PRGs using Venn analysis. (B) Kyoto Encyclopedia of Genes and Genomes pathway enrichment analysis of PRDEGs was visualized using a bubble plot. (C) The NLRP3 pathway was a canonical pyroptosis pathway. (D, F and H) Representative images of IF staining for NLRP3, caspase-1$^+$/TUNEL$^+$, and GSDMD in penile corpus cavernosum, respectively. (E, G and I) Semi-quantitative data of NLRP3, caspase-1$^+$/TUNEL$^+$ index and GSDMD expression as relative fluorescence intensity in penile corpus cavernosum, respectively. (J, L and N) Representative images of IF staining for NLRP3, caspase-1 and GSDMD in HUVECs, respectively. (K, M and O) Semi-quantitative data of NLRP3, caspase-1 and GSDMD expression as relative fluorescence intensity in HUVECs, respectively. There were three replicates in these experiments. $^{\#}$P<0.05 compared with the Control group. *P<0.05 compared with the CRD or LPS group. $^{\&}$P<0.05 compared with the LPS + MT group. MT, melatonin; NLRP3, NLR family pyrin domain containing 3; HUVECs, human umbilical vein endothelial cells; DEGS, differentially expressed genes; PRDEGs, pyroptosis-related DEGs; IF, immunofluorescence; GSDMD, gasdermin D; CRD, circadian rhythm disruption; LPS, lipopolysaccharide; LD, low dosage; HD, high dosage.

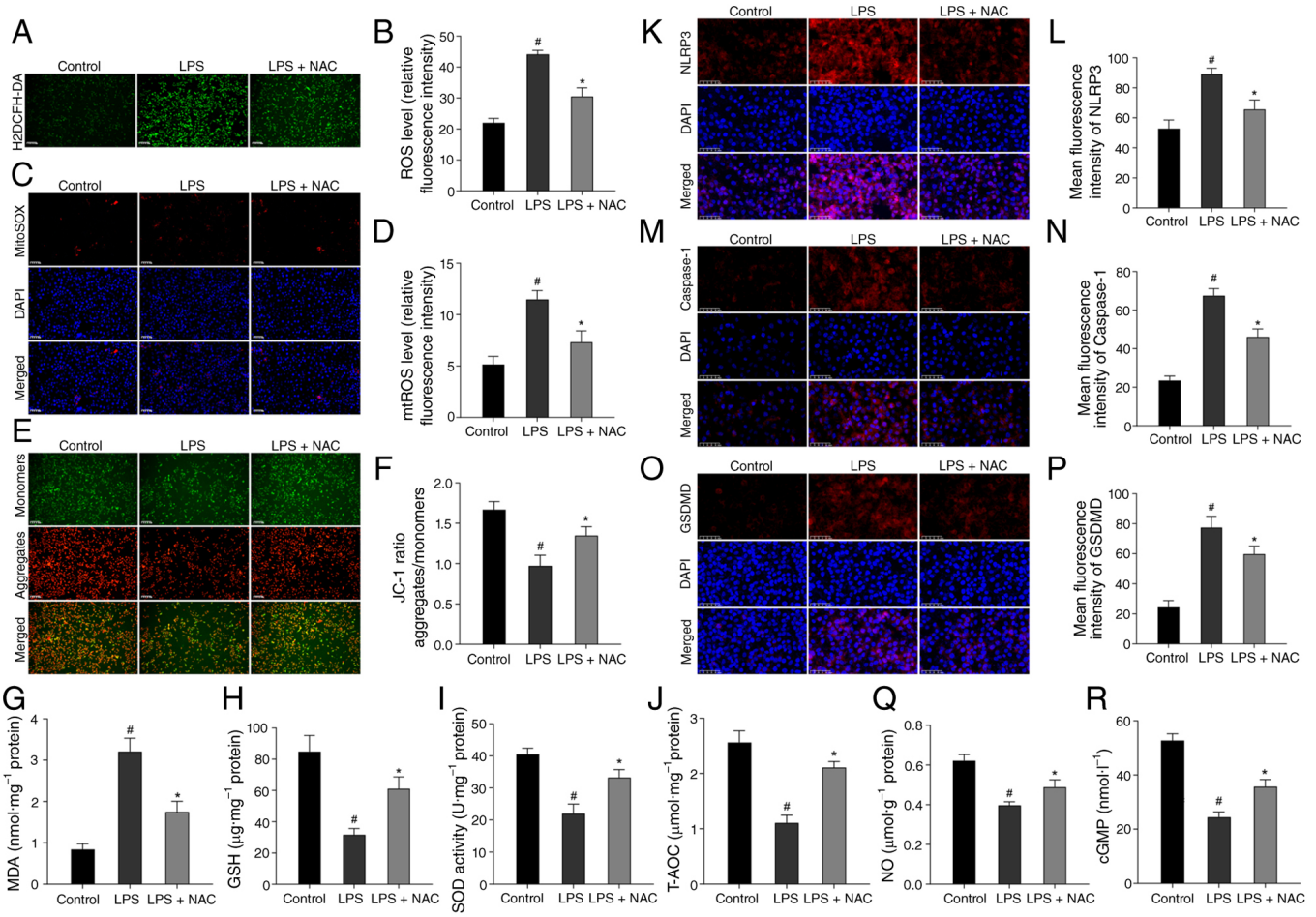

Figure 7. Antioxidative stress reduces NLRP3-mediated pyroptosis in HUVECs. (A) Representative images of H2DCFH-DA staining for ROS in HUVECs. (B) Semi-quantitative data of ROS level as relative fluorescence intensity in HUVECs. (C) Representative images of MitoSOX Red staining for mtROS in HUVECs. (D) Semi-quantitative data of mtROS level as relative fluorescence intensity in HUVECs. (E) Representative images of JC-1 staining for MMP in HUVECs. (F) Semi-quantitative data of MMP as a relative JC-1 ratio in HUVECs. (G-J) Levels of MDA, GSH, as well as SOD activity and T-AOC were measured in HUVECs, respectively. (K, M and O) Representative images of immunofluorescence staining for NLRP3, caspase-1 and GSDMD in HUVECs, respectively. (L, N and P) Semi-quantitative data of NLRP3, caspase-1 and GSDMD expression as relative fluorescence intensity in HUVECs, respectively. (Q and R) NO content and cGMP content in HUVECs, respectively. There were three replicates in these experiments. #P<0.05 compared with the control group; *P<0.05 compared with the LPS group. NLRP3, NLR family pyrin domain containing 3; HUVECs, human umbilical vein endothelial cells; ROS, reactive oxygen species; mtROS, mitochondrial ROS; MMP, mitochondrial membrane potential; MDA, malondialdehyde; GSH, reduced glutathione; SOD, superoxide dismutase; T-AOC, total antioxidant capacity; GSDMD, gasdermin D; NO, nitric oxide; cGMP, cyclic guanosine monophosphate; LPS, lipopolysaccharide.

Anti-oxidative stress reduces NLRP3-mediated pyroptosis in HUVECs. N-Acetyl-L-cysteine (NAC), an amino acid derivative of glutathione and cysteine, serves as a potent scavenger of ROS (40) and plays a crucial role in cellular antioxidant stress (41). To evaluate the inhibitory effect of NAC on LPS-induced NLRP3 activation, 10 mM NAC was pretreated for 3 h before LPS intervention in HUVECs. Initially, the impact of NAC on LPS-treated HUVECs was assessed. LPS induced a significant redox imbalance, that significantly elevated oxidative stress markers (ROS, mtROS and MDA) and decreased antioxidant parameters (MMP, GSH, SOD and T-AOC), all of which were partially reversed by NAC treatment (Fig. 7A-J), suggesting the ability of anti-oxidative stress.

Subsequently, it was explored whether the anti-oxidative effect of NAC could influence CRD-induced pyroptosis. As expected, LPS-treated HUVECs presented elevated pyroptosis activation, as indicated by increased expression of NLRP3, caspase-1 and GSDMD; however, this activation was partially reversed by NAC (Fig. 7K-P), suggesting that NAC reduced CRD-induced pyroptosis by inhibiting oxidative stress.

Furthermore, the endothelial function was also evaluated, that the endothelial function indicators of NO and cGMP in LPS-treated HUVECs were significantly decreased, however, these reductions were partially reversed by NAC (Fig. 7Q and R).

These data confirmed that NAC mitigated LPS-induced endothelial impairment by reducing oxidative stress to curb NLRP3-mediated pyroptosis, highlighting the central role of the oxidative stress-pyroptosis axis. In conclusion, all these proved that CRD-induced ED by inhibiting oxidative stress mediated pyroptosis via Nrf2/HO-1 axis, which was also the core therapeutic mechanism of MT.

Discussion

The present study aimed to elucidate the pathological mechanisms underlying CRD-induced ED and to further reveal the

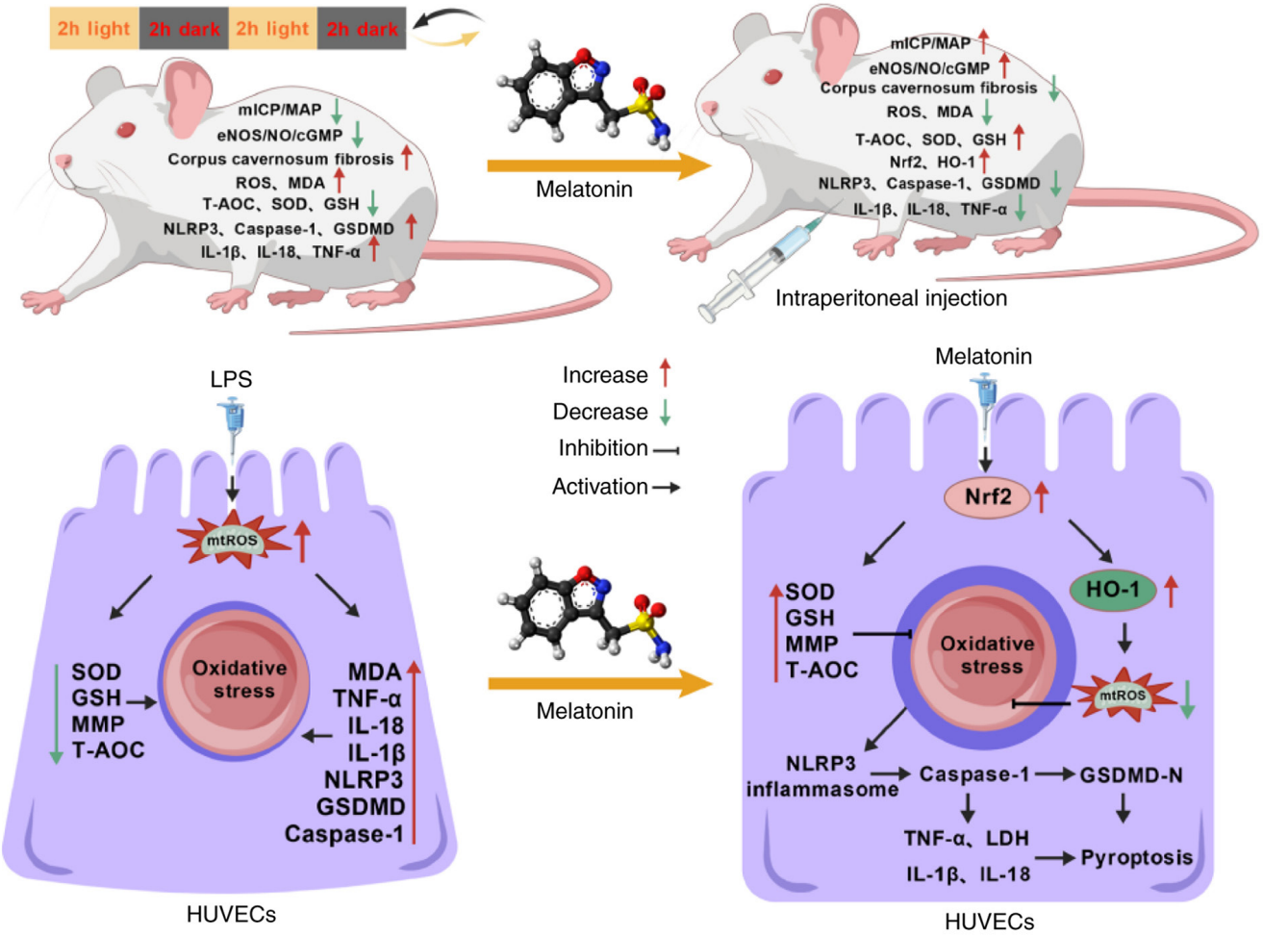

Figure 8. Summary of the therapeutic effect of MT on CRD-induced ED via suppression of oxidative stress-mediated pyroptosis through the Nrf2/HO-1 axis. MT, melatonin; CRD, circadian rhythm disruption; ED, erectile dysfunction; Nrf2, nuclear factor erythroid 2-related factor 2; HO-1, heme oxygenase 1; ICP, intracavernous pressure; mICP, maximum intracavernous pressure; MAP, mean arterial pressure; MDA, malondialdehyde; GSH, reduced glutathione; SOD, superoxide dismutase; T-AOC, total antioxidant capacity; LPS, lipopolysaccharide; ROS, reactive oxygen species; mtROS, mitochondrial ROS; MMP, mitochondrial membrane potential; NLRP3, NLR family pyrin domain containing 3; GSDMD, gasdermin D; eNOS, endothelial nitric oxide synthase; NO, nitric oxide; cGMP, cyclic guanosine monophosphate.

molecular basis of MT-mediated amelioration of this process. The principal findings of the present study demonstrated that CRD impaired erectile function in rats, suppressed the key eNOS-NO-cGMP signaling pathway, and caused severe microstructural damage to the penile corpus cavernosum. These structural and functional deficits were closely associated with elevated oxidative stress and increased pyroptosis. MT treatment successfully reversed all of the aforementioned changes. Mechanistically, it was demonstrated that CRD impaired endothelial function and induced pyroptosis through an oxidative stress-triggered cascade, leading to ED. By contrast, MT interrupted this cascade by activating the Nrf2/HO-1 signaling axis, thereby alleviating oxidative stress and pyroptosis, restoring endothelial integrity, and rescuing erectile function (Fig. 8). Based on these findings, the following sections integrate the current results with the existing literature to clarify the interrelationships among CRD, ED, oxidative stress and pyroptosis, while exploring the molecular mechanisms underlying the action of MT.

CRD and ED. The circadian rhythm represents a fundamental intrinsic timekeeping system (42). Epidemiological and clinical studies have consistently shown that CRD exposures, such as shift work (43), frequent time-zone changes (44) and chronic sleep loss (45), are strongly associated with an increased risk of ED, a finding also confirmed by the authors' previous studies (9,10). Based on direct *in vivo* and *in vitro* evidence, the present study establishes CRD as an independent risk factor for ED, thereby providing direct implications for understanding the high prevalence of ED among shift workers and other high-risk populations. The physiological process of erection critically depends on the NO-mediated vasodilatory signaling pathway within penile endothelial cells (11). The current investigation reveals that CRD substantially impairs the activity of this central eNOS-NO-cGMP pathway, which constitutes the direct molecular foundation of ED pathogenesis (46). Notably, beyond the disruption of this crucial signaling axis, the deeper pathophysiological consequences of CRD extend to substantial tissue structural damage and programmed cell death. These observations prompted a crucial investigation into the specific downstream pathways through which CRD mediates its damaging effects.

CRD and oxidative stress. The circadian rhythm system and cellular redox state maintain a sophisticated bidirectional

interplay (47). CRD disrupts this coordination, resulting in both overproduction and inefficient clearance of ROS (48). At the molecular level, core circadian components directly regulate the expression of numerous genes involved in antioxidant defense; however, CRD leads to the dysregulation of these genes, thereby increasing susceptibility to oxidative stress (49). Concurrently, oxidative stress products (for example, ROS) can feed back and impair the function of circadian rhythm proteins (for example, PER and EZH2), forming a vicious cycle (50). At the physiological level, CRD disrupts metabolism under the control of the circadian rhythm (for example, glycolysis and lipophagy). This metabolic reprogramming elevates oxidative byproducts (for example, ROS), while the capacity for their clearance is compromised due to CRD, collectively promoting oxidative stress (51). In the present study, penile corpus cavernosum tissue from rats with CRD displayed clear signs of oxidative stress; the current data strongly support a model in which oxidative stress acts as a critical link between CRD and downstream pathological injury. Furthermore, having identified oxidative stress as the central pathway in the therapeutic effect of MT on CRD-induced ED through transcriptomic analysis, it was next sought to elucidate how MT mediates its antioxidant protection at the molecular level.

MT inhibits oxidative stress via the Nrf2/HO-1 pathway. Nrf2 is a master transcriptional regulator of cellular antioxidant responses (52). Under physiological conditions, Nrf2 is constitutively bound to Keap1, localizes in the cytoplasm, and undergoes continuous proteasomal degradation (53). During oxidative stress, Nrf2 dissociates from Keap1 and translocates to the nucleus (54), where it binds to antioxidant response elements (AREs) (55) and initiates the transcription of antioxidant genes, including the critical cytoprotective enzyme HO-1 (56). HO-1 exerts potent antioxidant and cytoprotective effects by catalyzing the degradation of heme into biliverdin, carbon monoxide and free iron (57). Core circadian rhythm proteins regulate the expression and activity of Nrf2, generating circadian oscillations in cellular antioxidant capacity (58); Nrf2 knockout attenuates the rhythmicity of circadian genes while inducing aberrant oscillations in stress-response genes (59). Moreover, CRD impairs the time-giving function of the circadian rhythm, preventing pre-activation of antioxidant defenses prior to peak oxidative stress, thereby compromising defensive capacity when it is most needed (58). Ultimately, a vicious cycle emerges: CRD causes Nrf2 dysfunction and impairs antioxidant capacity, while accumulated ROS further disrupts circadian rhythm operation (60). Exogenous MT has been shown to activate the Nrf2 pathway and reduce oxidative stress in various models (61-63). The current data demonstrate that MT mediates its antioxidant activity by activating the Nrf2/HO-1 axis, the central transcriptional regulator of endogenous antioxidant responses, thus rebuilding cellular antioxidant capacity and counteracting CRD-induced oxidative damage.

Oxidative stress and pyroptosis: Downstream effector targets. If oxidative stress acts as an upstream event, what is its downstream effector target? In recent years, pyroptosis has been recognized as a key mechanism in the pathogenesis of multiple organ injuries (64). Pyroptosis is a novel form of inflammatory programmed cell death. The present study is the first, to the best of our knowledge to show the activation of NLRP3-mediated pyroptosis in a CRD-induced ED model. The mechanisms to establish the causal relationship between oxidative stress and pyroptosis in the present model were systematically analyzed. First, it was observed that MT alleviates pyroptosis by suppressing oxidative stress. This suggests an association between these processes. When Nrf2 was inhibited, the protection was abolished. This confirmed that Nrf2-dependent antioxidant activity is indispensable for preventing pyroptosis. The present data support that MT inhibits NLRP3-mediated pyroptosis mainly by activating Nrf2/HO-1 and reducing oxidative stress. This is shown by the reversal of MT's effects by the ROS scavenger NAC. However, Nrf2 may also directly suppress NLRP3 inflammasome activation through non-antioxidant mechanisms. Some studies have shown that Nrf2 can downregulate NLRP3 transcriptionally by binding to AREs in its promoter (65-67).

Nrf2 has also been reported to interact physically with NLRP3 or its upstream regulators (for example, TXNIP) and inhibit inflammasome assembly (68,69). In the present study, the possibility that MT-activated Nrf2 directly represses NLRP3 activation cannot be excluded. Future studies with Nrf2 mutants that keep transcriptional activity but lack antioxidant capacity, or chromatin immunoprecipitation assays to examine Nrf2 binding to the NLRP3 promoter, would clarify the roles of antioxidant-dependent and direct pathways.

Core innovations and clinical translational value. The core innovations of the present study are reflected in the following three aspects: i) First report of the therapeutic effect of MT on CRD-induced ED: Although MT has shown protective effects in diabetic ED and neurogenic ED models, its effect on CRD-related ED has never been investigated. The present study is the first to demonstrate that MT significantly improves erectile function in CRD rats, restoring the ICP/MAP ratio and preserving the eNOS-NO-cGMP pathway. i) First revelation of the 'oxidative stress-pyroptosis' axis in CRD-related ED: Previous mechanistic studies on ED have not linked CRD with the oxidative stress-pyroptosis axis. The present study is the first to establish that CRD triggers NLRP3-mediated pyroptosis through oxidative stress, and that MT interrupts this cascade via Nrf2/HO-1 activation, representing a completely new molecular pathway in iii) CRD-induced ED. Clinical translational value: CRD-related ED is a modern lifestyle-associated condition affecting shift workers, frequent travelers, and individuals with chronic sleep deprivation. These patients often have contraindications to PDE5is (for example, due to nitrate use for cardiovascular diseases) or suboptimal responses because of endothelial dysfunction. As an endogenous, low-toxicity, multi-target agent, MT represents a promising alternative or adjunctive therapy. The present study provides a strong preclinical rationale for future clinical trials evaluating MT supplementation in CRD-exposed populations with ED.

There are certain limitations to the present study. First, the *in vitro* experiments were performed using HUVECs rather than corpus cavernosum endothelial cells (CCECs). These two cell types differ in tissue origin, phenotype and physiological function; HUVECs may not fully recapitulate the *in vivo*

pathophysiological state of the corpus cavernosum. Future studies should use primary CCECs for validation.

Second, while the present study measured mitochondrial ROS and membrane potential, key indicators of mitochondrial oxidative stress, it is recognized that a more comprehensive assessment of mitochondrial homeostasis would strengthen the mechanistic understanding. Mitochondrial quality control involves not only redox balance but also dynamic changes in morphology (fusion/fission), biogenesis and mitophagy. Future studies should examine mitochondrial ultrastructure using transmission electron microscopy to visualize cristae integrity and swelling. Additionally, markers of mitochondrial biogenesis (PGC-1α, NRF1 and TFAM) and mitophagy (Parkin, PINK1 and LC3B) would help determine whether MT promotes the removal of damaged mitochondria or enhances the generation of healthy ones. It has been previously demonstrated that MT preserves mitochondrial function in various oxidative stress models by promoting PINK1/Parkin-dependent mitophagy (70). It would be of great interest to test whether similar mechanisms operate in CRD-induced ED. The current findings provide a strong foundation for such future investigations, which has been added as a key direction in the authors' ongoing studies.

Third, although programmed cell death pathways (pyroptosis, apoptosis and necroptosis) dynamically interact and may lead to integrated processes such as PANoptosis, pyroptosis was only assessed in endothelial cells. Markers of apoptosis (caspase-3), ferroptosis (GPX4), or necroptosis (RIPK3) were not systematically detected. Therefore, a comprehensive understanding of the individual contributions and crosstalk among different cell death modalities under pathological conditions is lacking.

Fourth, regarding the detection of pyroptosis, total GSDMD protein expression and caspase-1/TUNEL double staining were only assessed, without measuring the gold-standard indicators, including the cleaved N-terminal fragment of GSDMD (GSDMD-N). Thus, the conclusions are based primarily on NLRP3 and caspase-1 activation and morphological changes. Future studies should include these additional endpoints to provide more definitive evidence of pyroptosis.

In conclusion, it was demonstrated that CRD-induced ED by triggering an oxidative stress-pyroptosis cascade. Conversely, MT treatment effectively counteracts this pathology by activating the Nrf2/HO-1 pathway to suppress oxidative stress, thereby attenuating NLRP3-mediated pyroptosis and ultimately restoring erectile function. These results provide the first systematic evidence for the central role of the oxidative stress-pyroptosis axis in CRD-induced ED, establishing a solid theoretical foundation for MT as a promising therapeutic strategy for CRD-related ED.

Acknowledgements

Not applicable.

Funding

The present study was supported by the National Nature Science Foundation of China (grant nos. 82360295 and 82560562), the Guizhou Provincial Basic Research Program (Natural Science) program [grant no. QianKeHeJiChu-zk(2025)MianShang457], the Science and Technology Foundation Project of Guizhou Provincial Health Commission (grant no. gzwkj2024-150), the Doctor Start-up Fund of Affiliated Hospital of Guizhou Medical University (grant no. gyfybsky-2023-03) and the Affiliated Hospital of Guizhou Medical University 2025 Research Education and Research Feedback in Teaching Project (grant no. gyfykj-2025-y24).

Availability of data and materials

The data generated in the present study may be found in the Gene Expression Omnibus under accession number PRJNA1466509 or at the following URL: http://www.ncbi.nlm.nih.gov/bioproject/1466509.

Authors' contributions

QYa, WL and QYu conceptualized the study, wrote the original draft, and wrote, reviewed and edited the manuscript. JS and LY contributed to data curation and formal analysis. JQ and XW were involved in methodology. CG participated in investigation. FS and TL contributed to study conceptualization, were responsible for funding acquisition and reviewed and edited the manuscript and confirm the authenticity of all the raw data. All authors read and approved the final version of the manuscript.

Ethics approval and consent to participate

The animal protocols were approved by the Animal Ethics Committee of Guizhou Medical University (approval no. 2402989; Guiyang, China).

Patient consent for publication

Not applicable.

Competing interests

The authors declare that they have no competing interests.

References

1. Maestre-Lorén F, Castillo-Garayoa JA, López-I-Martín X, Sarquella-Geli J, Andrés A and Cifre I: Psychological distress in erectile dysfunction: The moderating role of attachment. Sex Med 9: 100436, 2021.
2. Salonia A, Bettocchi C, Boeri L, Capogrosso P, Carvalho J, Cilesiz NC, Cocci A, Corona G, Dimitropoulos K, Gül M, *et al*: European association of urology guidelines on sexual and reproductive health-2021 update: Male sexual dysfunction. Eur Urol 80: 333-357, 2021.
3. Samidurai A, Xi L, Das A and Kukreja RC: Beyond erectile dysfunction: cGMP-specific phosphodiesterase 5 inhibitors for other clinical disorders. Annu Rev Pharmacol Toxicol 63: 585-615, 2023.
4. Brock GB, McMahon CG, Chen KK, Costigan T, Shen W, Watkins V, Anglin G and Whitaker S: Efficacy and safety of tadalafil for the treatment of erectile dysfunction: Results of integrated analyses. J Urol 168: 1332-1336, 2002.
5. Ruan W, Yuan X and Eltzschig HK: Circadian rhythm as a therapeutic target. Nat Rev Drug Discov 20: 287-307, 2021.
6. McAlpine CS and Swirski FK: Circadian influence on metabolism and inflammation in atherosclerosis. Circ Res 119: 131-141, 2016.

7. Terentes-Printzios D, Ioakeimidis N, Rokkas K and Vlachopoulos C: Interactions between erectile dysfunction, cardiovascular disease and cardiovascular drugs. Nat Rev Cardiol 19: 59-74, 2022.
8. Nguyen V, McGovern AM, Rojanasarot S, Patel DP, Bhattacharyya S, Hargens LM, Aworunse O and Hsieh TC: Patient out-of-pocket costs for guideline-recommended treatments for erectile dysfunction: A medicare cost modeling analysis. Int J Impot Res 37: 45-50, 2025.
9. Li T, Jiang YT, Qi XZ, Chen P, Zhang JH, Luo F, Qiao J, Gu J, Du GS and Wang Q: Circadian disturbance induces erectile dysfunction by impairing endothelial function. Asian J Androl 26: 205-211, 2024.
10. Li T, Bai Y, Jiang Y, Jiang K, Tian Y, Wang Z, Ban Y, Liang X, Luo G and Sun F: Potential effect of the circadian clock on erectile dysfunction. Aging Dis 13: 8-23, 2022.
11. Mao Y, Zha Y, Zang Y, Gao Y, Sun J, Liu Y, Wang Z, Wei Z, Wang M and Yang Y: Isorhamnetin improves diabetes-induced erectile dysfunction in rats through activation of the PI3K/AKT/eNOS signaling pathway. Biomed Pharmacother 177: 116987, 2024.
12. Oyama Y, Bartman CM, Bonney S, Lee JS, Walker LA, Han J, Borchers CH, Buttrick PM, Aherne CM, Clendenen N, *et al*: Intense light-mediated circadian cardioprotection via transcriptional reprogramming of the endothelium. Cell Rep 28: 1471-1484.e11, 2019.
13. Maiese K: Diabetes mellitus and glymphatic dysfunction: Roles for oxidative stress, mitochondria, circadian rhythm, artificial intelligence, and imaging. World J Diabetes 16: 98948, 2025.
14. Wang X, Bian Y, Zhang R, Liu X, Ni L, Ma B, Zeng R, Zhao Z, Song X and Liu C: Melatonin alleviates cigarette smoke-induced endothelial cell pyroptosis through inhibiting ROS/NLRP3 axis. Biochem Biophys Res Commun 519: 402-408, 2019.
15. Fang Y, Tian S, Pan Y, Li W, Wang Q, Tang Y, Yu T, Wu X, Shi Y, Ma P and Shu Y: Pyroptosis: A new frontier in cancer. Biomed Pharmacother 121: 109595, 2020.
16. Zhang KJ, Wu Q, Jiang SM, Ding L, Liu CX, Xu M, Wang Y, Zhou Y and Li L: Pyroptosis: A new frontier in kidney diseases. Oxid Med Cell Longev 2021: 6686617, 2021.
17. Akbal A, Dernst A, Lovotti M, Mangan MSJ, McManus RM and Latz E: How location and cellular signaling combine to activate the NLRP3 inflammasome. Cell Mol Immunol 19: 1201-1214, 2022.
18. Wang Y, Yuan H, Shen D, Liu S, Kong W, Zheng K, Yang J and Ge L: Artemisinin attenuated ischemic stroke induced pyroptosis by inhibiting ROS/TXNIP/NLRP3/Caspase-1 signaling pathway. Biomed Pharmacother 177: 116894, 2024.
19. Bhattacharya S, Patel KK, Dehari D, Agrawal AK and Singh S: Melatonin and its ubiquitous anticancer effects. Mol Cell Biochem 462: 133-155, 2019.
20. Pandi-Perumal SR, BaHammam AS, Brown GM, Spence DW, Bharti VK, Kaur C, Hardeland R and Cardinali DP: Melatonin antioxidative defense: Therapeutical implications for aging and neurodegenerative processes. Neurotox Res 23: 267-300, 2013.
21. Ashrafizadeh M, Najafi M, Kavyiani N, Mohammadinejad R, Farkhondeh T and Samarghandian S: Anti-inflammatory activity of melatonin: A Focus on the role of NLRP3 inflammasome. Inflammation 44: 1207-1222, 2021.
22. Sahan A, Akbal C, Tavukcu HH, Cevik O, Cetinel S, Sekerci CA, Sener TE, Sener G and Tanidir Y: Melatonin prevents deterioration of erectile function in streptozotocin-induced diabetic rats via sirtuin-1 expression. Andrologia 52: e13639, 2020.
23. Chen Z, Zhai J, Ma J, Chen P, Lin W, Zhang W, Xiong J, Zhang C and Wei H: Melatonin-primed mesenchymal stem cells-derived small extracellular vesicles alleviated neurogenic erectile dysfunction by reversing phenotypic modulation. Adv Healthc Mater 12: e2203087, 2023.
24. Schwartz MD, Wotus C, Liu T, Friesen WO, Borjigin J, Oda GA and de la Iglesia HO: Dissociation of circadian and light inhibition of melatonin release through forced desynchronization in the rat. Proc Natl Acad Sci USA 106: 17540-17545, 2009.
25. Ogo FM, Siervo GEML, de Moraes AMP, Machado KGB, Scarton SRDS, Guimarães ATB, Cecchini AL, Simão ANC, Mathias PCF and Fernandes GSA: Extended light period in the maternal circadian cycle impairs the reproductive system of the rat male offspring. J Dev Orig Health Dis 12: 595-602, 2021.
26. Moustafa A: Effect of light-dark cycle misalignment on the hypothalamic-pituitary-gonadal axis, testicular oxidative stress, and expression of clock genes in adult male rats. Int J Endocrinol 2020: 1426846, 2020.
27. Yuan J, Lin H, Li P, Zhang R, Luo A, Berardinelli F, Dai Y and Wang R: Molecular mechanisms of vacuum therapy in penile rehabilitation: A novel animal study. Eur Urol 58: 773-780, 2010.
28. Kechin A, Boyarskikh U, Kel A and Filipenko M: cutPrimers: A new tool for accurate cutting of primers from reads of targeted next generation sequencing. J Comput Biol 24: 1138-1143, 2017.
29. Morris GM, Huey R and Olson AJ: Using AutoDock for ligand-receptor docking. Curr Protoc Bioinformatics Chapter 8: Unit 8.14, 2008.
30. Katchalski-Katzir E, Shariv I, Eisenstein M, Friesem AA, Aflalo C and Vakser IA: Molecular surface recognition: Determination of geometric fit between proteins and their ligands by correlation techniques. Proc Natl Acad Sci USA 89: 2195-2199, 1992.
31. Vakser IA: Long-distance potentials: An approach to the multiple-minima problem in ligand-receptor interaction. Protein Eng 9: 37-41, 1996.
32. Zhou C, Li J, Wu X and Liu F: Activation of spleen tyrosine kinase (SYK) contributes to neuronal pyroptosis and cognitive impairment in diabetic mice via the NLRP3/Caspase-1/GSDMD signaling pathway. Exp Gerontol 198: 112626, 2024.
33. Livak KJ and Schmittgen TD: Analysis of relative gene expression data using real-time quantitative PCR and the 2(-Delta Delta C(T)) method. Methods 25: 402-408, 2001.
34. Haspel JA, Chettimada S, Shaik RS, Chu JH, Raby BA, Cernadas M, Carey V, Process V, Hunninghake GM, Ifedigbo E, *et al*: Circadian rhythm reprogramming during lung inflammation, Nat Commun 5: 4753, 2014.
35. Ryzhikov M, Ehlers A, Steinberg D, Xie W, Oberlander E, Brown S, Gilmore PE, Townsend RR, Lane WS, Dolinay T, *et al*: Diurnal rhythms spatially and temporally organize autophagy. Cell Rep 26: 1880-1892.e6, 2019.
36. Yu Z, Wu D, Shi T, Chen D, Feng H, Chen H, Lin H, Sun L and Liu W: Melatonin attenuates spinal cord injury by regulating ferroptosis through the Nrf2/HO-1/GPX4 pathway. Mol Neurobiol 62: 15530-15549, 2025.
37. Asghar MA, Wan B, Li L, Zhang J, Tang S, Han H, Yang Y, Chu L, Zhang Q, Zhang X and Zhao Q: Micronutrient antioxidant supplementation alleviates valproic acid-induced oxidative stress and male infertility via the NRF2/HO-1 pathway. Redox Biol 85: 103685, 2025.
38. Song G, Wang J, Liu J and Ruan Y: Dimethyl fumarate ameliorates erectile dysfunction in bilateral cavernous nerve injury rats by inhibiting oxidative stress and NLRP3 inflammasome-mediated pyroptosis of nerve via activation of Nrf2/HO-1 signaling pathway. Redox Biol 68: 102938, 2023.
39. Liu P, Lu Z, Liu L, Li R, Liang Z, Shen M, Xu H, Ren D, Ji M, Yuan S, *et al*: NOD-like receptor signaling in inflammation-associated cancers: From functions to targeted therapies. Phytomedicine 64: 152925, 2019.
40. Wood JPM, Chidlow G, Wall GM and Casson RJ: N-acetylcysteine amide and di-N-acetylcysteine amide protect retinal cells in culture via an antioxidant action. Exp Eye Res 248: 110074, 2024.
41. Santus P, Signorello JC, Danzo F, Lazzaroni G, Saad M and Radovanovic D: Anti-inflammatory and anti-oxidant properties of N-acetylcysteine: A fresh perspective. J Clin Med 13: 4127, 2024.
42. Dollish HK, Tsyglakova M and McClung CA: Circadian rhythms and mood disorders: Time to see the light. Neuron 112: 25-40, 2024.
43. Zheng Z, Pan J, Chen Z, Gao P, Gao J, Jiang H and Zhang X: The association between shift work, shift work sleep disorders and premature ejaculation in male workers. BMC Public Health 24: 1772, 2024.
44. Desmet L, Thijs T, Segers A, Verbeke K and Depoortere I: Chronodisruption by chronic jetlag impacts metabolic and gastrointestinal homeostasis in male mice. Acta Physiol (Oxf) 233: e13703, 2021.
45. Petzke F, Heppner C, Mbulamberi D, Winkelmann W, Chrousos GP, Allolio B and Reincke M: Hypogonadism in Rhodesian sleeping sickness: Evidence for acute and chronic dysfunction of the hypothalamic-pituitary-gonadal axis. Fertil Steril 65: 68-75, 1996.
46. Smimmo M, Casale V, Casillo GM, Mitidieri E, d'Emmanuele di Villa Bianca R, Bello I, Schettino A, Montanaro R, Brancaleone V, Indolfi C, *et al*: Hydrogen sulfide dysfunction in metabolic syndrome-associated vascular complications involves cGMP regulation through soluble guanylyl cyclase persulfidation. Biomed Pharmacother 174: 116466, 2024.

47. Paeng SK, Wi SD, Chae HB, Bae SB, Phan KAT, Kim MG, Yun DJ, Kim WY, McClung CR and Lee SY: NTRC mediates the coupling of chloroplast redox rhythm with nuclear circadian clock in plant cells. Mol Plant 18: 468-484, 2025.
48. Huang S, Zhang W, Ba M, Xuan S, Huang D, Qi D, Pei X, Lu D and Li Z: Chronic jet lag disrupts circadian rhythms and induces hyperproliferation in murine lacrimal glands via ROS accumulation. Invest Ophthalmol Vis Sci 66: 12, 2025.
49. Wang H, Guo M, Ren B, Zhang H, Zhang J, Qiao R, Qian L, Zhu J, Zhang S, Su W, *et al*: Circadian control of hepatic ischemia/reperfusion injury via HSD17B13-mediated autophagy in hepatocytes. J Hepatol 83: 750-767, 2025.
50. Zhang HY, Li KY, Wang YL, Wei CJ, Gao YX, Ren-Zhou, Zhong YB, Yin ZJ and Ren DL: ROS regulates circadian rhythms by modulating Ezh2 interactions with clock proteins. Redox Biol 81: 103526, 2025.
51. Zhou R, Li K, Hu X, Fan S, Gao Y, Xue X, Bu Y, Zhang H, Wang Y, Wei C, *et al*: Sleep deprivation activates a conserved lactate-H3K18la-RORα axis driving neutrophilic inflammation across species. Adv Sci (Weinh) 12: e04028, 2025.
52. Nishikawa S, Inoue Y, Hori Y, Miyajima C, Morishita D, Ohoka N, Hida S, Makino T and Hayashi H: Anti-inflammatory activity of kurarinone involves induction of HO-1 via the KEAP1/Nrf2 pathway. Antioxidants (Basel) 9: 842, 2020.
53. Xian P, Hei Y, Wang R, Wang T, Yang J, Li J, Di Z, Liu Z, Baskys A, Liu W, *et al*: Mesenchymal stem cell-derived exosomes as a nanotherapeutic agent for amelioration of inflammation-induced astrocyte alterations in mice. Theranostics 9: 5956-5975, 2019.
54. Zhang T, Wu P, Budbazar E, Zhu Q, Sun C, Mo J, Peng J, Gospodarev V, Tang J, Shi H and Zhang JH: Mitophagy reduces oxidative stress via Keap1 (kelch-like epichlorohydrin-associated protein 1)/Nrf2 (nuclear factor-E2-related factor 2)/PHB2 (prohibitin 2) pathway after subarachnoid hemorrhage in rats. Stroke 50: 978-988, 2019.
55. Kopacz A, Klóska D, Proniewski B, Cysewski D, Personnic N, Piechota-Polańczyk A, Kaczara P, Zakrzewska A, Forman HJ, Dulak J, *et al*: Keap1 controls protein S-nitrosation and apoptosis-senescence switch in endothelial cells. Redox Biol 28: 101304, 2020.
56. Wu CT, Deng JS, Huang WC, Shieh PC, Chung MI and Huang GJ: Salvianolic acid C against acetaminophen-induced acute liver injury by attenuating inflammation, oxidative stress, and apoptosis through inhibition of the Keap1/Nrf2/HO-1 signaling. Oxid Med Cell Longev 2019: 9056845, 2019.
57. O'Rourke SA, Shanley LC and Dunne A: The Nrf2-HO-1 system and inflammaging. Front Immunol 15: 1457010, 2024.
58. Pekovic-Vaughan V, Gibbs J, Yoshitane H, Yang N, Pathiranage D, Guo B, Sagami A, Taguchi K, Bechtold D, Loudon A, *et al*: The circadian clock regulates rhythmic activation of the NRF2/glutathione-mediated antioxidant defense pathway to modulate pulmonary fibrosis. Genes Dev 28: 548-560, 2014.
59. Horton NS, Copple IM, Vasilaki A, Jackson MJ, McArdle A and Pekovic-Vaughan V: P 089-NRF2/KEAP1-mediated antioxidant defence pathway regulates skeletal muscle circadian clock function. Free Radic Biol Med 108: S48, 2017.
60. Tamaru T, Hattori M, Ninomiya Y, Kawamura G, Varès G, Honda K, Mishra DP, Wang B, Benjamin I, Sassone-Corsi P, *et al*: ROS stress resets circadian clocks to coordinate pro-survival signals. PLoS One 8: e82006, 2013.
61. Jing H, Sun X, Li M, Peng J, Gu X and Xiong J: Exogenous melatonin activating nuclear factor E2-related factor 2 (Nrf2) pathway via melatonin receptor to reduce oxidative stress and apoptosis in antler mesenchymal stem cells. Molecules 27: 2515, 2022.
62. Guo S, Yang J, Qin J, Qazi IH, Pan B, Zang S, Lv T, Deng S, Fang Y and Zhou G: Melatonin promotes in vitro maturation of vitrified-warmed mouse germinal vesicle oocytes, potentially by reducing oxidative stress through the Nrf2 pathway. Animals (Basel) 11: 2324, 2021.
63. Zhang Y, Cong P, Tong C, Jin H, Liu Y and Hou M: Melatonin pretreatment alleviates blast-induced oxidative stress in the hypothalamic-pituitary-gonadal axis by activating the Nrf2/HO-1 signaling pathway. Life Sci 280: 119722, 2021.
64. Zhao X, Xie J, Duan C, Wang L, Si Y, Liu S, Wang Q, Wu D, Wang Y, Yin W, *et al*: ADAR1 protects pulmonary macrophages from sepsis-induced pyroptosis and lung injury through miR-21/A20 signaling. Int J Biol Sci 20: 464-485, 2024.
65. Tao W, Hu Y, Chen Z, Dai Y, Hu Y and Qi M: Magnolol attenuates depressive-like behaviors by polarizing microglia towards the M2 phenotype through the regulation of Nrf2/HO-1/NLRP3 signaling pathway. Phytomedicine 91: 153692, 2021.
66. Zhang C, Zhao M, Wang B, Su Z, Guo B, Qin L, Zhang W and Zheng R: The Nrf2-NLRP3-caspase-1 axis mediates the neuroprotective effects of Celastrol in Parkinson's disease. Redox Biol 47: 102134, 2021.
67. Arioz BI, Tastan B, Tarakcioglu E, Tufekci KU, Olcum M, Ersoy N, Bagriyanik A, Genc K and Genc S: Melatonin attenuates LPS-induced acute depressive-like behaviors and microglial NLRP3 inflammasome activation through the SIRT1/Nrf2 pathway. Front Immunol 10: 1511, 2019.
68. Song X, Fan S, Gao Y, Ma A, Zhang X, Zhou Z, Zheng Y, Du L and Zhu X: Swietenolide inhibits the TXNIP/NLRP3 pathways via Nrf2 activation to ameliorate cognitive dysfunction in diabetic mice. Neuropharmacology 267: 110312, 2025.
69. Wang CY, Xu Y, Wang X, Guo C, Wang T and Wang ZY: Dl-3-n-butylphthalide inhibits NLRP3 inflammasome and mitigates Alzheimer's-like pathology via Nrf2-TXNIP-TrX axis. Antioxid Redox Signal 30: 1411-1431, 2019.
70. Yi S, Zheng B, Zhu Y, Cai Y, Sun H and Zhou J: Melatonin ameliorates excessive PINK1/Parkin-mediated mitophagy by enhancing SIRT1 expression in granulosa cells of PCOS. Am J Physiol Endocrinol Metab 319: E91-E101, 2020.